R/V Kronprins Haakon

15-31 October 2020

Tromsø-Longyearbyen

CAGE20-6 Cruise Report

Pore-fluid pressure and heat flow surveys along the Vestnesa Ridge, west-Svalbard continental margin

Chief scientist: Andreia Plaza-Faverola

Captain: Johnny Peder Hansen

1.   Introduction

CAGE20-6 cruise on board R/V Kronprins Haakon to the west Svalbard margin is the third research expedition of the SEAMSTRESS project – Tectonic stress effects on Arctic methane seepage (2019-2023). The project and therefor the cruise is primarily funded by the Tromsø Research Foundation (TFS) and the Research Council of Norway (RCN project number 287865) through their starting grant schemes. The project and cruises are also supported by the Department of Geosciences and the Center for Arctic gas hydrates, environment and climate at UiT – The Arctic University of Norway.

SEAMSTRESS is investigating how the stress generated by regional processes in Arctic margins (e.g., mid-ocean ridge spreading, glacial advance and retreat, tides, gravitational forcing) affect pore fluid pressure and seepage.

Cruise CAGE20-6 focusses on the Vestnesa Ridge fluid flow system (figure 1) and the main cruise objective is to search for spatial pressure and temperature variations along the ridge. We use the Ifremer Piezometer for in-situ pore fluid pressure measurements and the newly acquired UiT heat flow probe for temperature/conductivity measurements and heat flow calculations.

The in-situ pressure survey along the Vestnesa Ridge started in 2019 during CAGE19-3 cruise [*Knies et al.*, 2019; *Sultan et al.*, 2020] the first SEAMSTRESS expedition) and continues this year. This year we collected pressure data from 4 piezometer stations and heat flow data from 27 stations. In addition chirp and sonar data as well as gravity cores are available from each super station.

The regional heat flow survey is intended as a large project to complete the survey by Crane et a., started in the 90s [*Crane et al.*, 1991]. The obtained heat flow data will allow further constraining the dynamics of the bottom simulating reflection (BSR) along the Vestnesa Ridge [e.g., *Plaza-Faverola et al.*, 2017] and further constraining spreading rates of the Molloy and Knipovich mid- ocean ridges [e.g., *Johnson et al.*, 2015]
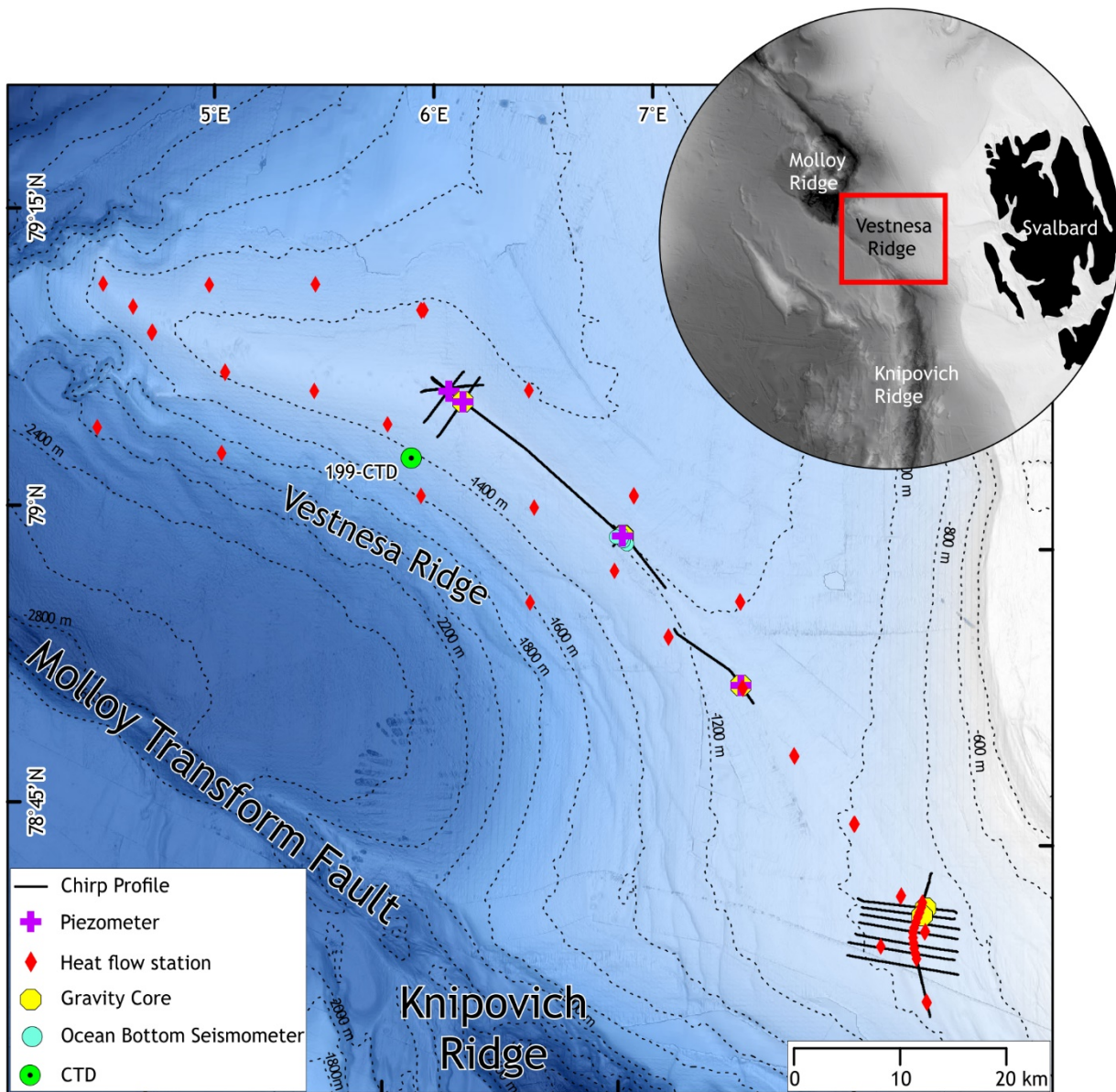
Figure 1 Study area and locations of the data acquired during CAGE20-6

2. Scientific crew

Andreia Plaza-Faverola, Researcher CAGE-UiT (Cruise leader)

Sunil Vadakkepuliyambatta, Researcher CAGE-UiT (Leader acoustics, data managing and responsible Heat Flow)

Nabil Sultan, Research Ifremer (responsible Piezometer data)

Stephan Ker, Research Ifremer (responsible Ocean Bottom Seismometer data)

Mickael Roudaut, technician Ifremer (Piezometer and OBSs)

Anthony Ferrant, technician Ifremer (Piezometer and OBSs)

Truls Holm, engineer UiT (Heat flow and gravity coring)

Jan Vidar Nordstrand, IMR (Acoustic instruments)

Roy Robertsen, IMR (Acoustic instruments)

Hanne Børsheim, IMR (Acoustic instruments)

Sunny Singhroha, Researcher CAGE-UiT (shifts cross-communication, data integration)

Frances Cooke, PhD student UiT (chirp data processing, gravity coring)

Przemyslaw Domel, PhD student UiT (sonar data processing, gravity coring)

Rémi Vachon, Post doc UiT (main gravity coring)

Hariharan Ramachandran, Post doc UiT (sonar data processing, gravity coring)

3.   Equipment

3.1   CTD

The CTD measures acoustic velocity, conductivity, temperature and other relevant oceanographic information based on sensors used in the device. Water column acoustic velocities from CTD measurements are used in the EK80 single-beam echosounder and EM302 multibeam echosounder for bathymetric mapping. The CTD instrument used on the cruise is the SBE11 plus from Seabird Scientific. The CTD system consists of the Seabird SBE 11 plus deck unit connected to bottle SBE32 carousel for water sampling. The CTD is equipped with the following sensors: 2 x SBE3 Temperature sensors (s/n: 4535 and 4306), 2 x SBE4 Conductivity sensors (s/n: 4386 and 2799), 2 x SBE43 oxygen sensors (s/n: 3947 and 3949), 1x PSA916 Altimeter (s/n: 73084), 1x pressure sensor (s/n: 141612), 1 x Wet Labs C-Star beam transmissometer (s/n: CST-2003 DR(420-461)), 1x Wet Labs ECO-AFL/FL Fluorometer (s/n: FLRTD-1547, FLRCDRTD-1930), and 1 x Biospherical PAR sensor (s/n: 70736) with Surface PAR (s/n: 20568) added. 2 pumps (s/n: 9378 and 9379) are used to make water run through these sensors. The CTD measures parameters at 44Hz and uses Seasave win 7.26.7.107 for data logging. SBE Data processing v. 7.26.7 is used for post-data processing. Figure 2 shows profile from different measurements at CTD location (Figure 2).
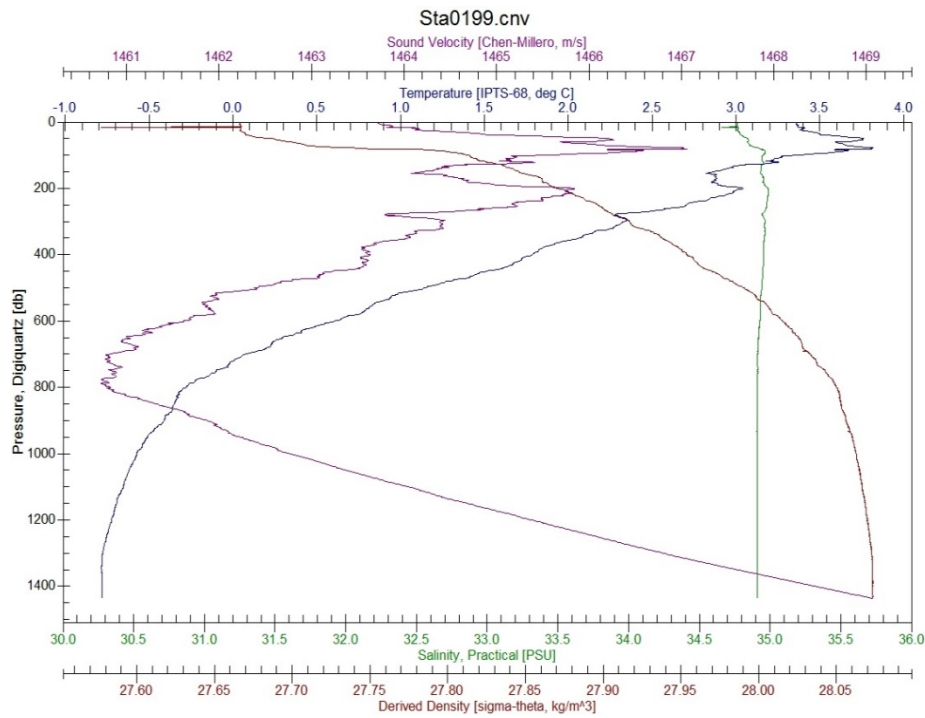
Figure 2: Temperature, density, sound velocity and salinity measured at CTD station 1.

3.2 Kongsberg SBP300 Sub-bottom profiler

The data were recorded using the hull-mounted Kongsberg SBP300 MK2 and software system version 1.6.6. The maximum depth of penetration is 100ms TWT (approximately 30 metres) over contourite drifts (Figure 3). The chirp pulse form is 'linear chirp up' with 30ms sweep length and frequencies between 2.5 and 7 kHz. The transmit power starts with a soft setting -30dB and gradually increases (over 2.5 minutes) to -5dB. The ping rate and bottom tracking is externally controlled by the EM302 multibeam system, and varies with depth. Typically at water depth of 1000m a ping interval of 4 seconds is suitable. Sample interval is 48 kHz with an acquisition time window of 500 ms. The vessel velocity is 4-5 knots while surveying and during transits 8 knots. The average trace (along track) interval for a 5 knot survey (ship speed we used) is approximately 10m.

The sweep function from the signal is removed using a matched filter based on autocorrelation of the Klauder wavelet. Gain correction is applied, which corrects for spherical loss of the acoustic pressure wave in the water column. Time variable gain is also applied prior to the logging of the processed sequence. The vertical resolution is 0.15m, using a sound velocity of 1500 m/s, typical of sea water and shallow sediments. The acquisition processing applies the envelope function to the data (instantaneous amplitude) which improves the signal-to-noise ratio. The signal phase of the data is removed and displays positive amplitudes only. This is the standard for interpretation of chirp data. The segy data, output from the Kongsberg acquisition system is in data format 4 byte IEEE float. The same file format is used while processing in Seismic Unix (SU). Files with the suffix '_UTMXXN' are files output from SU. The XY coordinates are stored in byte positions 73 and 77 and copied to 81 and 85. The data are projected to Universal Transverse Mercator zones (UTM), for which,

31N is the zone used for the data acquired in this survey. The UTM zone number can also be found in byte position 21 (CDP). The data are logged with varying delay recording time (delrt) to reduce file size in acquisition. When required, the data are shifted back to a constant delay recording time in SU. The range of the minimum and maximum time values are expanded, when final processing reveals a partial display of data, with data muted outside of the 500ms acquisition time window.

Interpretation

Horizons interpreted in Chirp data from survey CAGE19_3 were used to extend age estimates (Figure 3) acquired using data from the MARUM-MeBo-70 sediment drill rig and gravity core data [*Himmler et al.*, 2019; *Schneider et al.*, 2018] and Dessandier et al., in review.
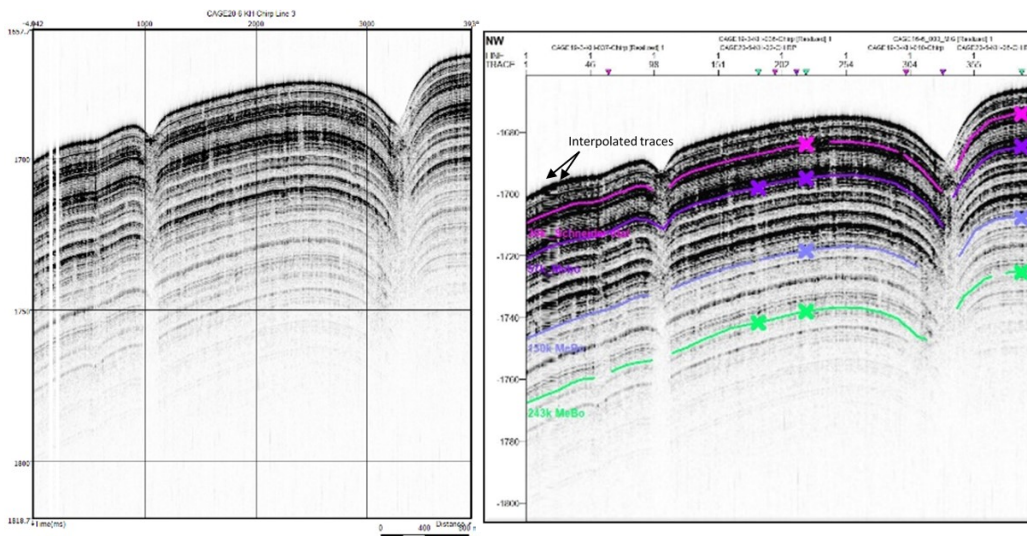

Figure 3: Example of sub-bottom profile data

3.3 EM302 Multibeam sonar data

We used EM302 multibeam system by Kongsberg to study seafloor and water column in the vicinity of Vestnesa Ridge. The system works by sending hundreds of electromagnetic pulses in horizontal swaths that travel through the seafloor, get reflected, and are subsequently received back. The frequency of electromagnetic beams sent is 30 kHz. Resolution of the system depends on the number of the beams shot and the area they ultimately cover at the seafloor (with increasing depth resolution decreases). For our survey, we used 432 beams, covering in total 90 degrees in angular resolution (45 degree each side from vertical position). So the horizontal resolution can be given as:

resolution=depth x tan(beam_range_per_side) / no_of_beams_per_side

We were conducting surveys in areas with depths ranging from 1200 m to about 2500 m. For 1200 m (depth of the crest at the east of Vestnesa Ridge), the horizontal resolution of the system with 216 beams per side covering 45 degrees equaled 5,55 m. Resolution in the direction of the ship traversal depends on the speed

of the ship and the depth of the water (greater depth requires more time between each pinging). The speed of pinging is controlled by the multibeam system itself and for the ship speed of 5 knots we have around 4 meter separation between each swath at the seabottom.

We get the information of the depth to the seafloor from the travel time of each beam. In addition, by studying the change of the signal strength when we receive back, we can identify density anomalies in the water column that indicate the presence of gas bubbles racing through the water.

All processing is done in QPS software: Qimera (bathymetry) and FMMidwater (water column) (Figure 4, 5). File extension *.all contains the bathymetry data; file extension *.wcd contains the water column data
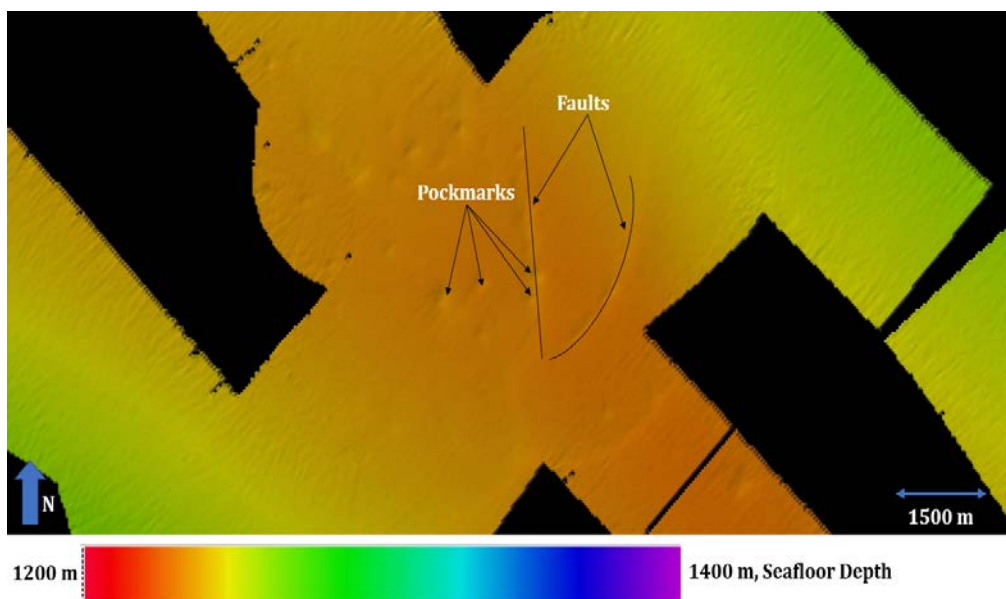

Figure 4: Bathymetry from Vestnesa Ridge (lat – 79°07'13.01"N, long – 6°07'03.07"E, water depth ~1237m). Image from Qimera Software.
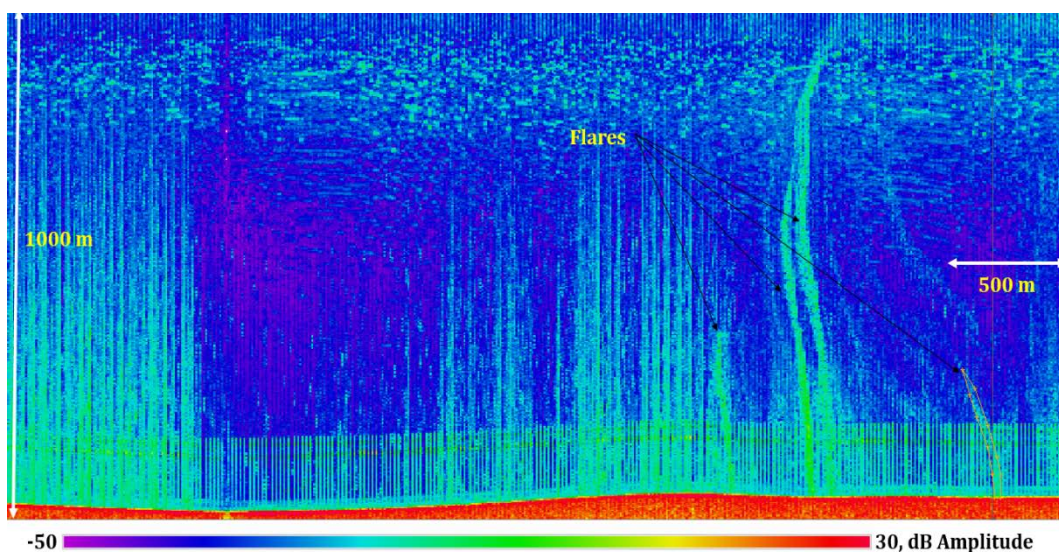
3.4   Gravity corer

UiT's gravity corer (GC) has a total weight of ~1000 kg. It consists of a 6 m long steel barrel with an inner diameter of 11 cm, a steel-mantled led weight at the top, and a core head with a core catcher at the bottom. For each deployment, a 5.95 m black plastic liner (pipe) with an outer diameter of 11 cm and inner diameter of 10 cm is inserted into the steel barrel. The gravity core is lifted horizontally by two slings attached to a crane while hooked up to the traction winch rope. The gravity core is lowered through the water column at 1m/s and further through the sediments by its own weight.

After retrieval, the plastic liners were manually cut into sections of up to 100 cm length, while taking care of the plastic sawdust (a significant amount of plastic is released form the cutting procedure; we collected as much as possible from the deck to avoid it going to the sea). The section ends were secured with plastic caps and the sections were labelled.

3.5   Heat flow Probe

To measure the in situ subsurface thermal regime and thermal conductivities of sediments, the FIELAX deep-sea heat flow probe is employed (Figure 6). The probe consists of a series of 22 thermistors and heating elements placed within a sensor string ~6.05 m long. The thermistors are places 0.26 cm apart and is designed for a temperature range of -2 to 60 ^{0}C with a resolution of 1 mK and accuracy of 2 mK after calibration. The sensor string is attached to a strength member, which bears the load while penetrating the sediments. The head section of the heat flow probe consists of data acquisition and power supply units. The whole probe weighs ~1100 kg and is rated for operation up to 6000 meters water depth.
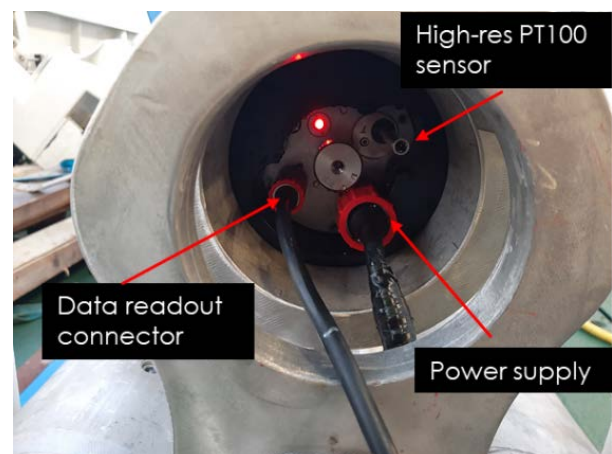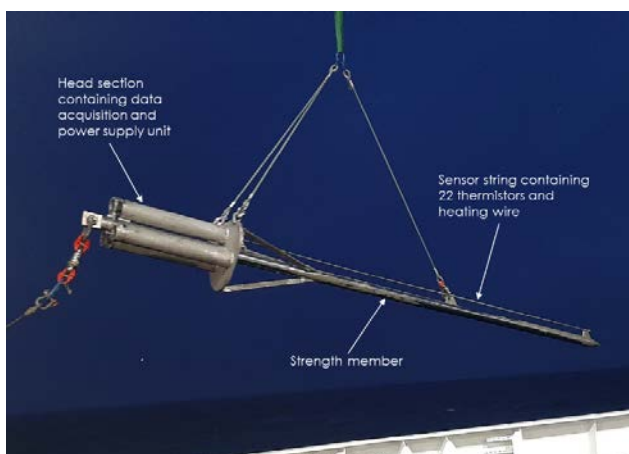
The data acquisition unit records the data from the sensor string and sends the heat pulse energy to the heating wires on the sensor string (Figure 6). It hosts a high-precision temperature sensor PT100, can measure tilt in two axes as well as the vertical acceleration. The pressure data from PT100, tilt, and vertical acceleration are used to configure the triggering of heat pulse and period of recording, whereas the temperature data from PT100 is used to calibrate the thermistors on the sensor string. In situ thermal gradients are calculated using the temperatures measured by the thermistors, whereas in situ thermal conductivity is estimated using the heat pulse method [*Lister et al.*, 1990], where the sensor string is heated up for 20 s and thermal conductivity is derived from the following temperature decay. The post-processing and quality control of the data was performed using Fellow software from Fielax, which estimates thermal gradients, thermal conductivity, and heat flow for each penetration.

The thermistors must be calibrated with temperature measurements from PT-100 sensor before each survey for accurate measurements. This was performed during the first deployment of the heat flow probe, where the tool was lowered to 1271 m water depth, where the temperature in the water column is constant over 10 m (data from CTD 199) and kept for 10 minutes. Calibration data is shown in the table below.

Sensor	Temp.(degC)	DeltaT
PT100	-0.7721	
S1	-0.8009	-0.0288
S2	-0.7640	0.0369
S3	-0.8202	-0.0562
S4	-0.8315	-0.0113
S5	-0.7788	0.0527
S6	-0.7994	-0.0206
S7	-0.7639	0.0355
S8	-0.7916	-0.0277
S9	-0.8437	-0.0521
S10	-0.8235	0.0202
S11	-0.7705	0.0530
S12	-0.7738	-0.0033
S13	-0.8354	-0.0616
S14	-0.7702	0.0652
S15	-0.7978	-0.0276
S16	-0.8221	-0.0243
S17	-0.7657	0.0564
S18	-0.7958	-0.0301
S19	-0.7812	0.0146
S20	-0.7875	-0.0063
S21	-0.7664	0.0211
S22	-0.7620	0.0044

Table 1 Temperatures measured at 22 thermistors on the sensor string and its variance with precision PT100 sensor on the data acquisition unit.

During CAGE20-6, in-situ temperatures were measured at 27 stations involving 83 successful penetrations (Figure 7). The main aims for the heat flow survey were to obtain high-resolution background heat flow measurements on the Vestnesa Ridge, and to identify fine-scale variations in thermal properties of sediments in the elongated depression North of Knipovich Ridge.
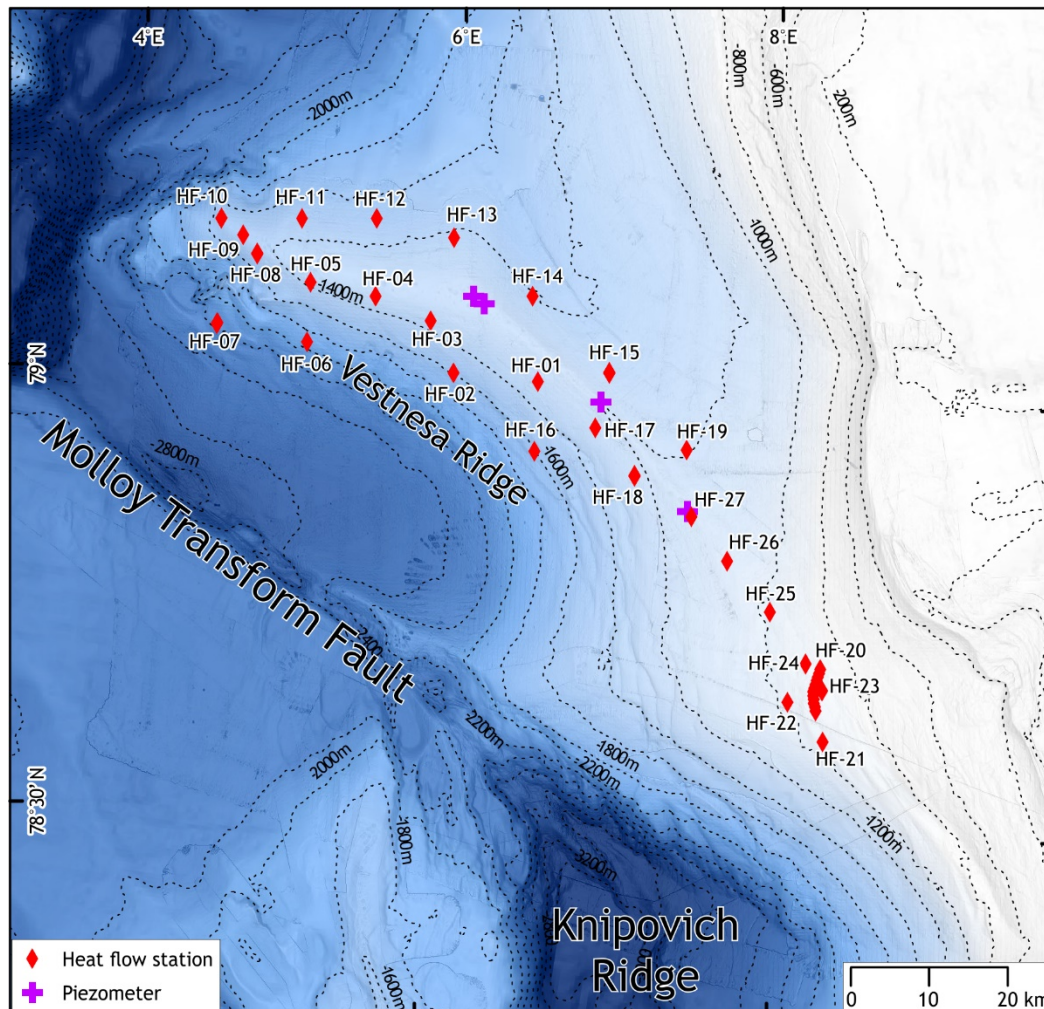
Figure 7 Overview of the heatflow stations during CAGE20-6. Stations 20-24 are at and around the elongated depression, whereas other stations were used to constrain the background heatflow over Vestnesa Ridge.

Two different styles of data acquisition were employed for achieving these goals. Over the Vestnesa Ridge, the heat flow probe was deployed over the starboard side of the vessel and allowed to penetrate the sediments at a winch speed of ~1.0 m/s. The tool was then kept stable for 15-20 minutes (to allow for temperature decay after frictional heating during penetration) before a heat pulse was released. The tool is kept on the seafloor for another 15-20 minutes to allow for the heat pulse to decay. The probe was then pulled out at a winch speed of ~0.2m/s to ~50 m above the seafloor and the ship moved to a nearby position ~50 m away. The probe was then allowed to penetrate again and record for 10-15 minutes. This process is repeated one more time before taking the tool up onboard. No heat pulse is triggered during the second and third penetrations. The last two penetrations were used to validate the thermal gradient

measured during the first penetration. At the elongated depression, north of Knipovich Ridge, a 'pogo-style' heat flow measurement was conducted (Figure 8). Here, the probe was kept stable within the sediments for 20 minutes before the heat pulse was triggered. The probe is then kept stable for another 20 minutes to allow for heat pulse decay. Then, the probe was pulled to and moved to the next station 500 m away and lifted above 50 m to release the next heat pulse before penetration. The procedure is then repeated (Figure 8).
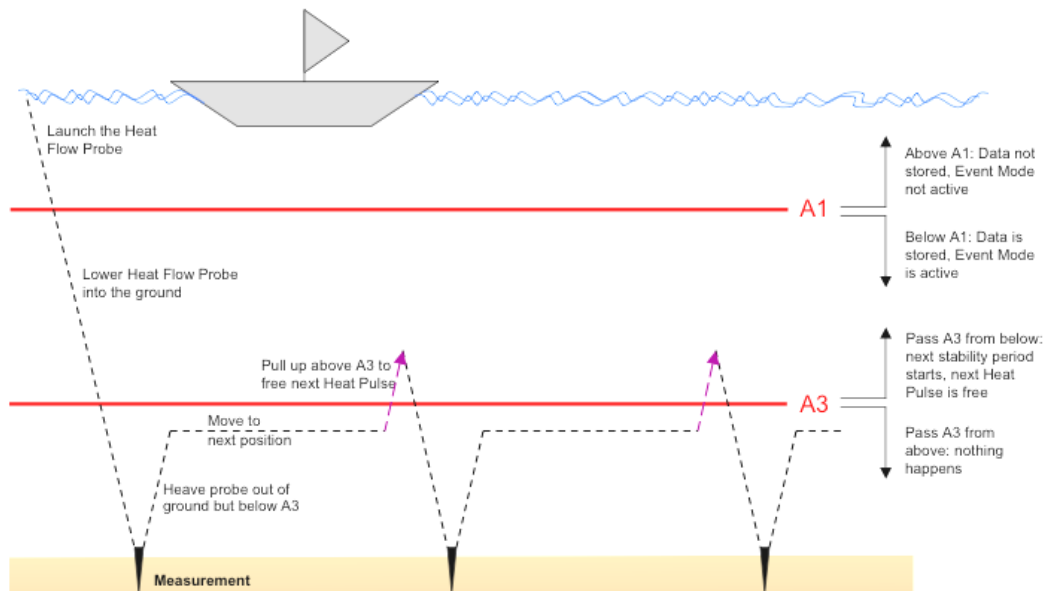

Figure 8 Overview of the "Pogo-Style" measurements with the heat flow probe.

During the measurements at both areas, the heat pulse was set to release while the probe was stable for 15-20 minutes, and the tilt was within 10^0 with fluctuations within 0.5^0, and acceleration fluctuations within 0.01 (A2). Recording of the data started during deployment and stopped after bringing the probe back onboard (A1). The distance limit for activating a second heat pulse (A3), was set at 100 dbar during the Vestnesa measurements and at 50 dbar for the measurements at elongated depression (Figure 8).

3.6 Ifremer Piezometer

The Ifremer piezometer is a free-fall device with a sediment-piercing lance attached to a recoverable instrument part (**Error! Reference source not found.**). It is ballasted with lead weights (up to 1000 kg) to penetrate a range of sediment types in water depths of up to 6000 m. The length of the lance used depends on the stiffness of the sediment with a maximum length of 12 meters. Pore pressures are measured relative to hydrostatic pressure at different ports on the 60 mm diameter lance using specially adapted differential pressure transducers connected to the pressure ports and the open seawater. The piezometer pore pressure sensors have an accuracy of ± 0.5 kPa. The piezometer lance is also equipped with temperature sensors located at the same level as the pore pressure sensors. Temperature sensors have an accuracy of 0.05 °C.
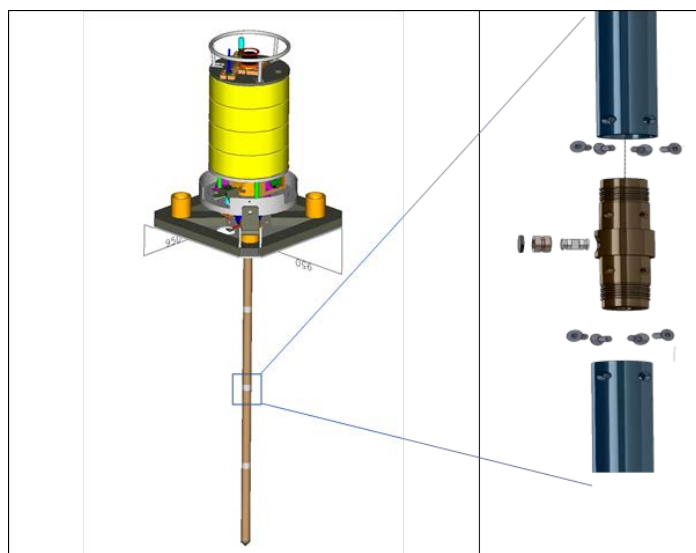
Figure 9   Schematic of the Ifremer Piezometer.

During this cruise two piezometers of 9.11 m length equipped with 9 temperature and 8 pressure sensors (**Error! Reference source not found.**) were used (during CAGE19-3 cruise only one piezometer was taken onboard). The first temperature sensor is in the water-column (around 0.5 m above the seabed) while the other 8 sensor depths are between 0.79 and 8.64 m (**Error! Reference source not found.**).

Section length (m)	Sensor names	Sensor depth (mbsf)
	T0	In the water column (around 0.5 m above the seabed)
0.75	T1, P1	0.79
0.75	T2, P2	1.59
1.50	T3, P3	3.14
1.50	T4, P4	4.69
1.50	T5, P5	6.24
0.75	T6, P6	7.04
0.75	T7, P7	7.84
0.75	T8, P8	8.64
Total lance length (cm)		9.11

Table 2 Piezometer characteristics and position of sensors.

We carried-out four deployments in the study area (Vestnesa ridge – offshore Svalbard) with recording periods between 2.75 and 3.5 days (**Error! Reference source not found.**). The aim is to determine the

hydraulic properties of the near-surface sediment and to characterize the in-situ hydraulic and thermal regimes.

Simplified names	Sites	# of sensors	Coordinates	Water depth (m)	Recording period (Time UTC)
STR2-PZ1	CAGE20-6-KH-12-PZM-01	8 P and 9 T	79° 7.242 N 6° 08.088 E	1234	20/10/2020 18:22 23/10/2020 19:52
STR2-PZ2	CAGE20-6-KH-04-PZM-01	8 P and 9 T	79° 0.285 N 6° 56.123 E	1207	21/10/2020 19:45 24/10/2020 19:09
STR2-PZ3	CAGE20-6-KH-12-PZM-02	8 P and 9 T	79° 6.747 N 6° 12.104 E	1228	23/10/2020 23:00 27/10/2020 10:17
STR2-PZ4	CAGE20-6-KH-04-PZM-02	8 P and 9 T	78° 52.891 N 7° 28.596 E	1127	25/10/2020 02:06 27/10/2020 18:46

Table 3 Piezometer names and recording periods; STR2 is short for SEAMSTRESS2.

3.7 Ifremer Ocean Bottom Seismometers

Ifremer short-period 4-component OBSs are MicrOBS from SERCEL (Figure 10): one hydrophone, a vertical geophone and two horizontal geophones. The sampling frequency is 1000 Hz (Table 4), the natural frequency of geophones is 4.5 Hz and the cut-off frequency of the hydrophone is 2Hz. In addition, a large band autonomous hydrophone (200 kHz) was installed on the piezometer PZ2 (79° 0.285; 6°56.123, 2020/10/21 at 19H45). The autonomy of this instrument was 5 hours. OBS locations, drift times, and technical details are summarized in tables 4-8.

MicrOBS Setup Parameters	
Sampling Frequency	1000 Hz
Hydro/geo Gain	20 dB / 26 dB (1x/2x)
Filter option	FIR2
Drift values (ms):	-9;-78;u;-13;5

Table 4 OBS setup parameters

Hyrdophone Setup Parameters	
Sampling Frequency	512kHz
Time shift (ms):	+50

Table 5 Hydrophone setup parameters

Mircrobs	Depth	Latitude	Longitude
OBS1	1196	78°59.86519	6°57.39578
OBS2	1196	79°00.02276	6°56.49431
OBS3	1137	79°00.12687	6°55.87014
OBS4	1208	79°00.37879	5°55.73538
OBS5	1201	79°00.20266	6°54.49714

Table 6 OBSs coordinates

Mircrobs	Synchro	Drift
OBS1	2020/10/20 11:44	2020/10/25 8:47:59
OBS2	2020/10/20 12:05	2020/10/25 12:07:59
OBS3	2020/10/20 12:20	/
OBS4	2020/10/20 12:30	2020/10/25 19:11:59
OBS5	2020/10/20 11:40	2020/10/25 19:15:00

Table 7 time synchronization

Mircrobs	Release
OBS1	2020/10/25 04:19
OBS2	2020/10/25 05:08
OBS3	2020/10/25 05:13
OBS4	2020/10/25 06:14
OBS5	2020/10/20 08:00

Table 8 time release

Figure 10   Ifremer Ocean Bottom Seismometers

4   Stations and data acquisition

Here we describe the investigated areas along the Vestnesa Ridge and the type of data acquired. All the surveys and stations are summarized in the Appendix tables. The investigations concentrated on 3 super stations (1, 4, 12 established during CAGE19-3 cruise).

4.1 Super station 12 - Turning point between the eastern and the western Vestnesa Ridge (VR) segments.

The western VR segment is inactive (in terms of seepage) with respect to the eastern VR (i.e., no acoustic flares recognized in sonar data over multiple annual visits to the area). A north-south trending fault appears to mark the transition between the eastern and the western Vestnesa ridge segments and it has been hypothesized that this is also an area marking a lateral change in the stress regime from strike slip dominated (in the non-seeping area) to tensile dominated (in the active seepage area) [*Plaza-Faverola and Keiding*, 2019]. We placed the piezometer at both sides of the main fault to investigate pore fluid pressures at both sides of the main fault zone (Figure 11). One gravity core was taken before 12-PZM02 deployment to assess the ease of penetration (Figure 12). A gravity and calypso cores were already taken near 12- PZM01 during CAGE19-3 cruise.
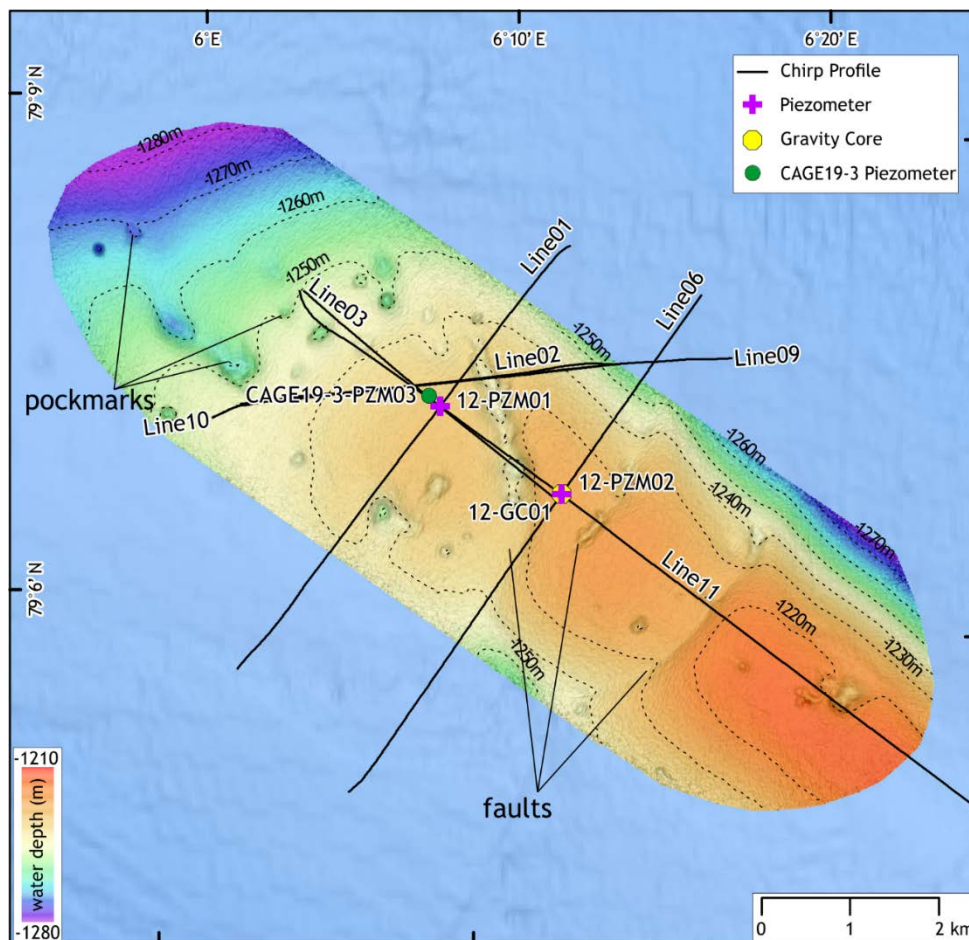

Figure 11 Location of surveys and data sites at super station CAGE20-6-KH-12. Two piezometer stations, one gravity core and 5 acoustic lines (sub-bottom profile and multi beam echosounder) were acquired in this area.
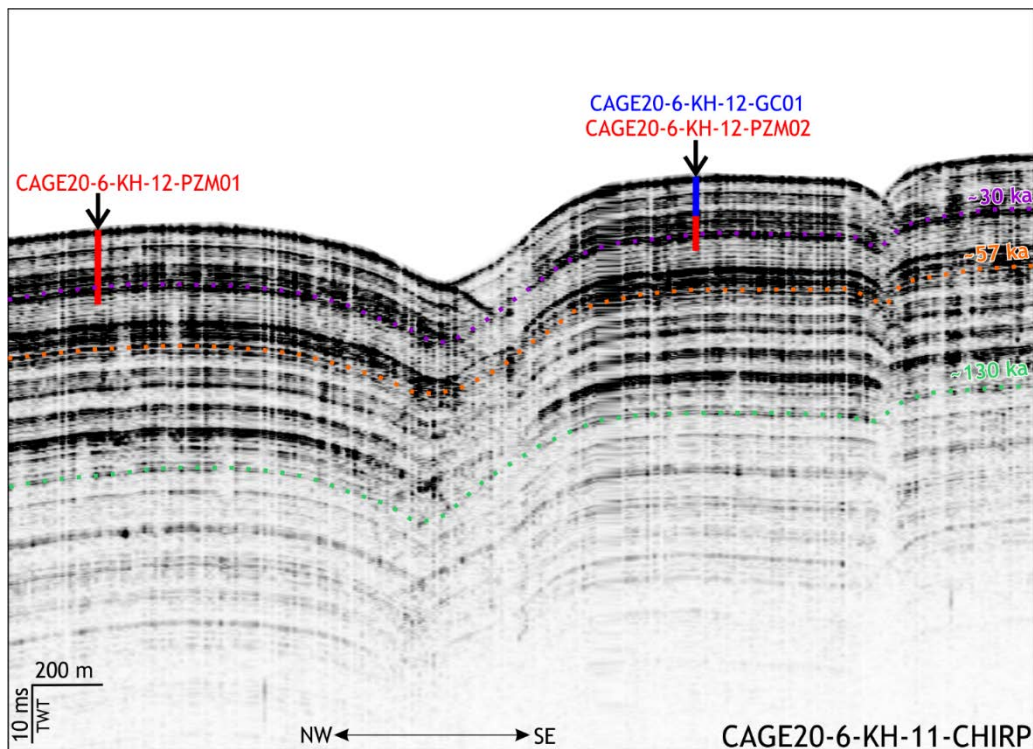
Figure 12 Location of CAGE20-6-KH-12-PZM1, CAGE20-6-KH-12-PZM2 and CAGE20-6-KH-12-GC01 on sub-bottom profile data.

Site CAGE20-6_KH_12_PZM1 (Str2-PZ1)

At site CAGE20-6_KH_12_PZM1, the piezometer Str2-PZ1 was deployed the 20/10/2020 to the west of Vestnesa ridge at water depth of 1234 m, west of the north-south oriented fault structure (Figure 11). Temperature and pore pressure variations during the installation of the piezometer are shown in Figure 13. Piezometer penetration compresses and shears the surrounding sediments under undrained conditions, thus generating excess pore-water pressure and heat development. The recorded data shown in Figure 13 indicate that the deployment was successful and the whole piezometer rod has penetrated the sediment between 18:22 and 18:23. The build-up pressure recorded by this piezometer is between 6 and 95 kPa (Figure 13). Besides, the temperature increases after the piezometer penetration due to the heat development (Figure 13).

Figure 13. Data from piezometer site Str2-PZ1: Temperature and pore pressure variations during the installation of the piezometer.

Once piezometer insertion stops, penetration-induced pressures and temperatures dissipate monotonically with time allowing to characterize the in-situ hydraulic and thermal regimes (Figure 14). The in-situ equilibrium temperature is reached 4 to 6 hours after the installation (Figure 13). However, the low hydraulic diffusivity of the sediment in the region prevents obtaining the in-situ equilibrium pore pressure after 3 days of measurement. The equilibrium in-situ pore pressure will be derived on land using a cavity expansion theory approach [*Sultan and Lafuerza*, 2013].

Figure 14. Data from piezometer site Str2-PZ1: Temperature and pore pressure versus time. The different colors indicate the depth below the seabed. Sensor depths are between 0.79 mbsf (blue curve) and 8.64 mbsf (red curve).

Site CAGE20-6_KH_12_PZM2 (Str2-PZ3)

At site Str2-PZ3, the piezometer was deployed the 23/10/2020 at around 2 km to the east of Str2-PZ1 (Figure 11). The water depth at this site is of 1234 m. Temperature and pore pressure variations during the installation of the piezometer are shown in Figure 15. The recorded data in 15 indicate that the deployment was successful and the whole piezometer rod has penetrated the sediment between 23:01 and 23:02. The build-up pressure recorded by this piezometer is between 7 and 102 kPa (Figure 16).
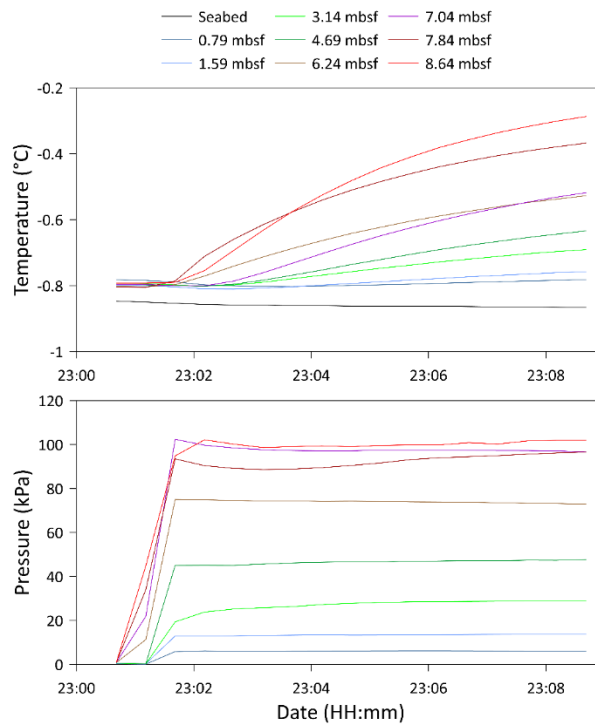
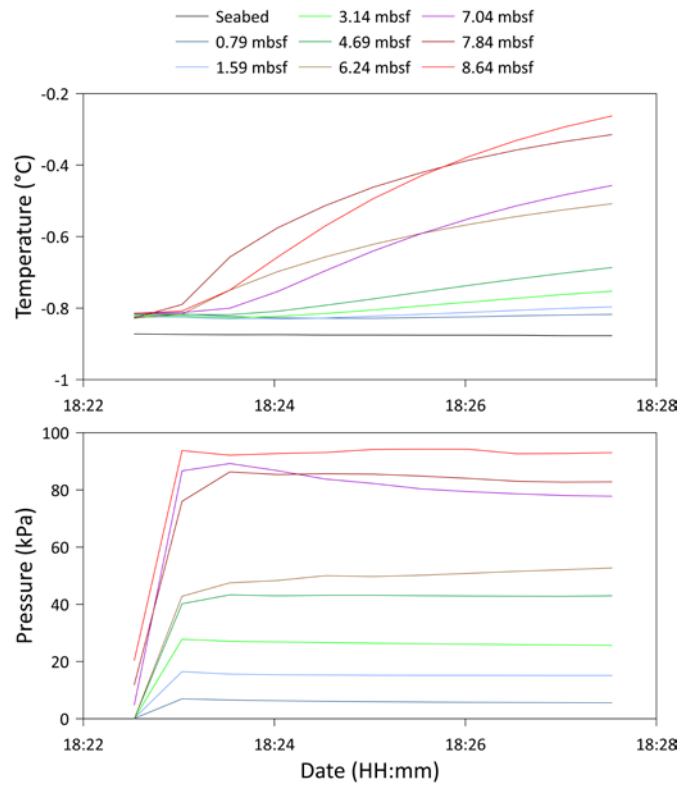*Figure 15. Data from piezometer site Str2-PZ3: Temperature and pore pressure variations during the installation of the piezometer.*
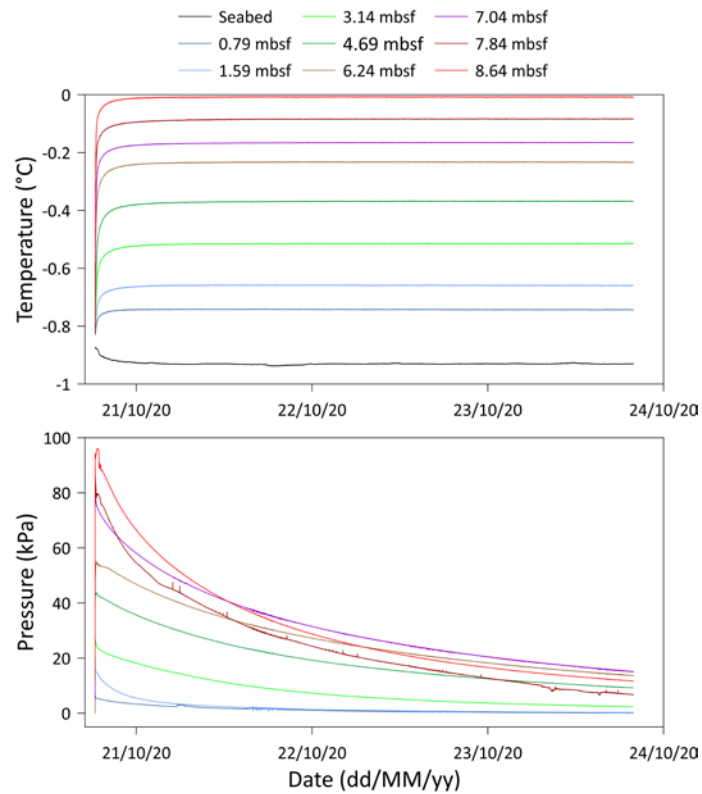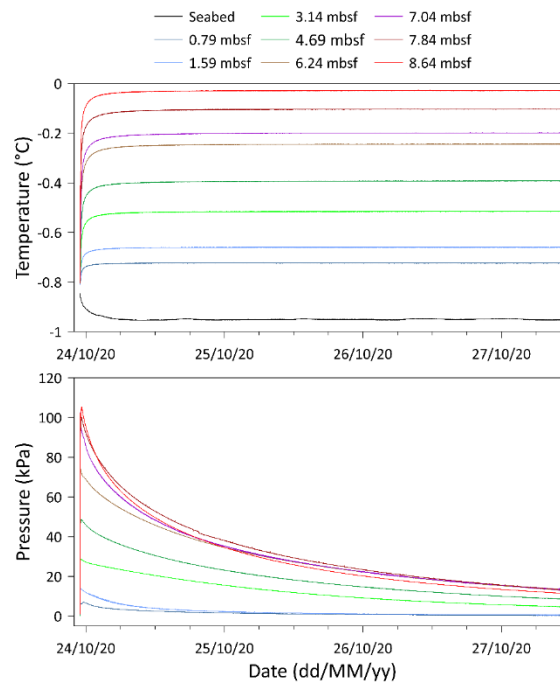

Figure 16. Data from piezometer site Str2-PZ3: Temperature and pore pressure versus time. The different colors indicate the depth below the seabed. Sensor depths are between 0.79 mbsf (blue curve) and 8.64 mbsf (red curve).

The pore pressure recorded by sensors P6 to P8 showed a fast decay of the pore pressure with respect to the P5 sensor, which is an indicator of a high hydraulic diffusivity of the sediment at P6 to P8 depths with respect to the sediment at P5 level (Figure 16).

4.2 Super station 4 - Eastern Vestnesa Ridge (VR) segment

This is the ridge segment where acoustic flares can be recognized in sonar data every year we visit the area. We placed the piezometer in two sites. The first site is at the northern rim of the Lomvi pockmark (Figure 17). Here we deployed 5 OBSs to study the potential relation between micro seismicity and piezometer signals. The other site is to the east of the first pockmark cluster along the VR crest (Figure 19). The aim here was to retrieve the background pressure for comparison with the background pressure from the other piezometer sites along the Vestnesa Ridge. One gravity core was takes before piezometer deployment to check penetration at each site (Figure 19).
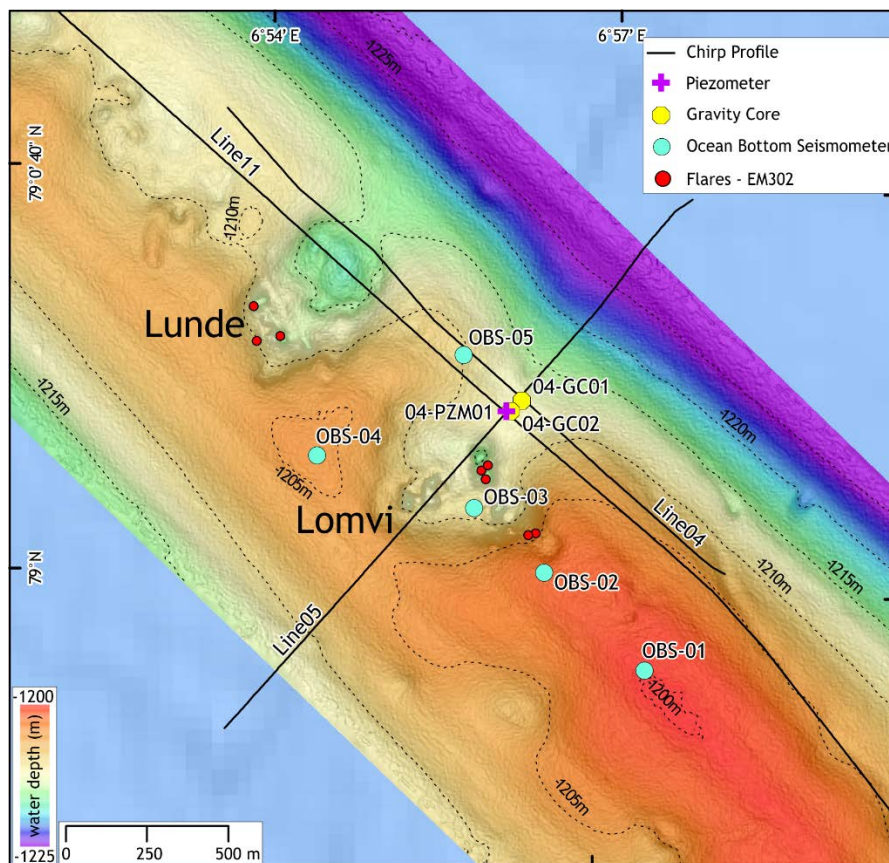
Figure 17 Bathymetry and experiment designs at site CAGE20-6-KH-04-PZM1. The area was survey with sub-bottom profiler and multi beam echosounder to ensure gas seepage and to select a safe area for deployment of the piezometer. Two gravity cores were attempted before final deployment. 5-OBS were driven down with a USBL and placed as accurately as possible in an array surrounding the piezometer.
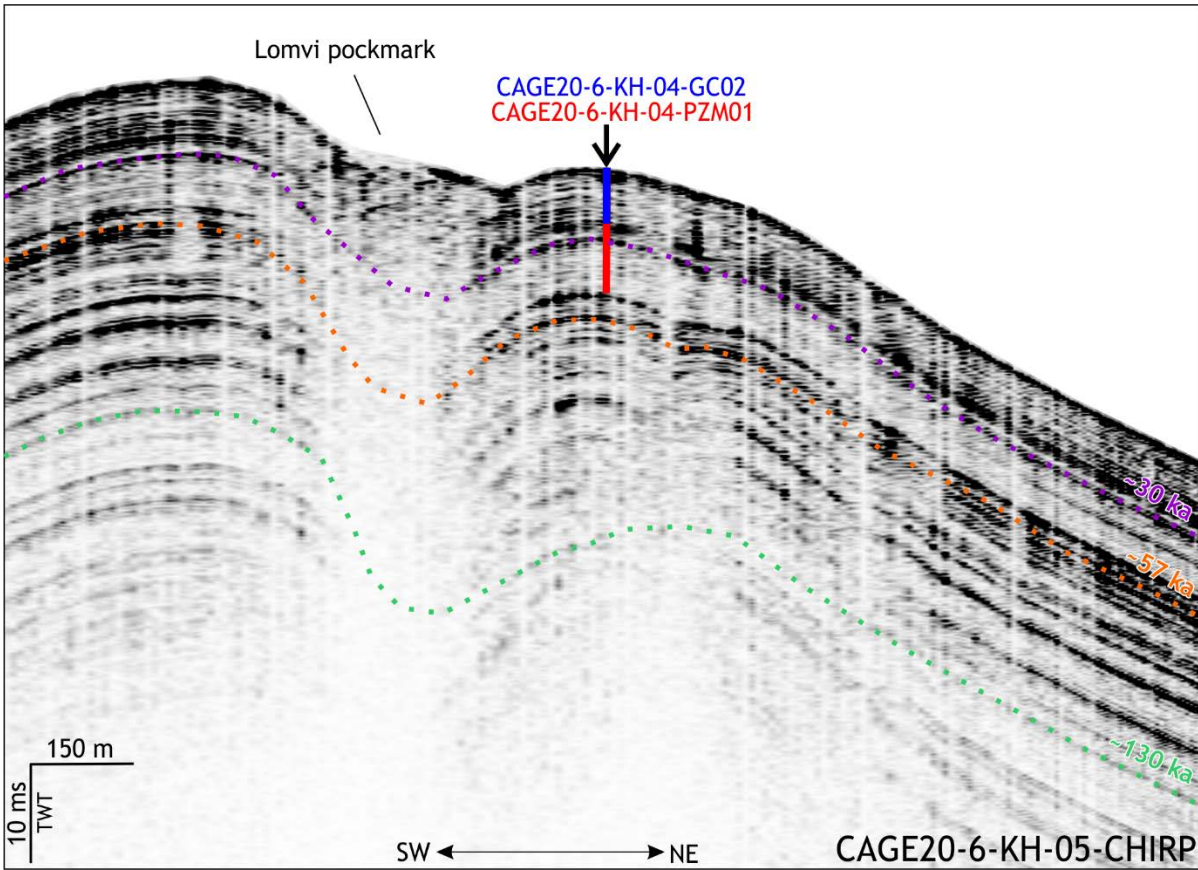
Figure 18 Sub bottom profile with the location of CAGE20-6-KH-04-GC03 and CAGE20-6-KH-04-PZM02.
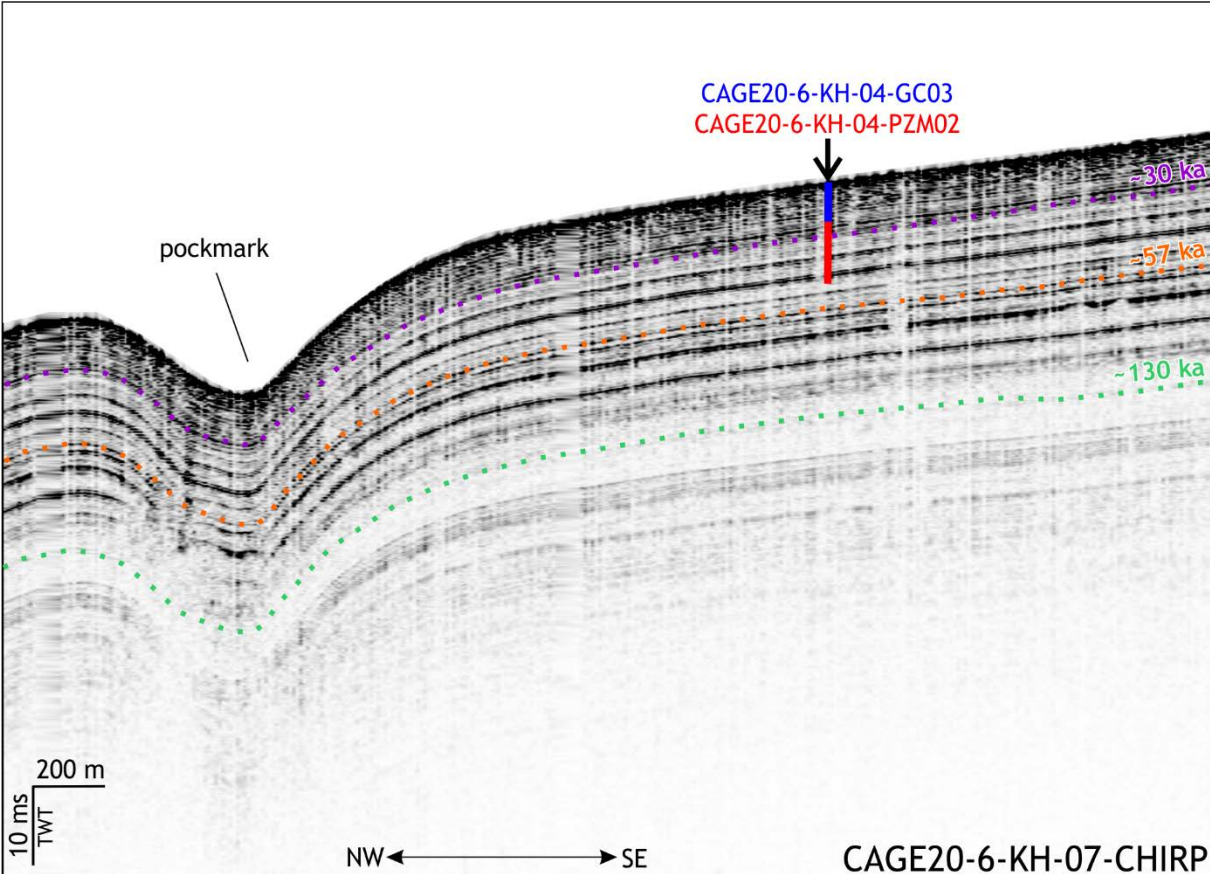
Figure 19 Sub bottom profile with the location of CAGE20-6-KH-04-GC03 and CAGE20-6-KH-04-PZM02.

Short-term OBSs experiment

We designed an experiment with an array of five short-period Ocean Bottom Seismometers to study the microseismicity that could be related to fluid activities (surface leakage or deep circulation) at the Lomvi pockmark. The five OBSs were carefully deployed around the pockmarks and the piezometer using the winch wire with a mounted USBL. Deployment of each OBS took 2 hours in average and recover one hour in average. Three instruments form a line with one instrument inside the pockmark (OBS3) and two instruments outside the pockmark with increasing distance (OBS1 and OBS2). Two instruments are located outside the pockmark with different azimuth with OBS5 close to the piezometer location (Figure 17). The picture below shows an example of an event identified in all the component of the 5 instrument.
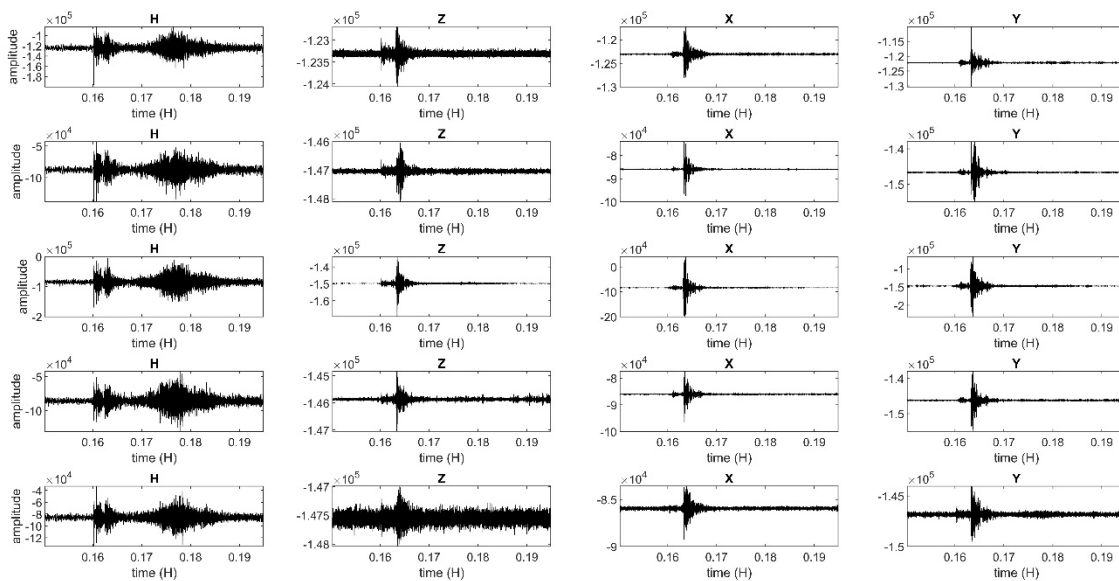

Figure 20 Event visible on all OBSs and all components – 2020/10/22 20H00

Site CAGE20-6_KH_04_PZM1 (Str2-PZ2)

At site Str2-PZ2, the piezometer was deployed the 21/10/2020 to the northeast of the Lomvi pockmark (Vestnesa ridge) at water depth of 1207 m (Figure 17). Temperature and pore pressure variations during the installation of the piezometer are shown in Figure 21. The recorded data shown in Figure 21 indicate that the deployment was successful and the whole piezometer rod has penetrated the sediment between 19:44 and 19:45. The build-up pressure recorded by this piezometer is between 10 and 130 kPa (Figure 22).The temperature data after the installation confirm the whole penetration of the piezometer.
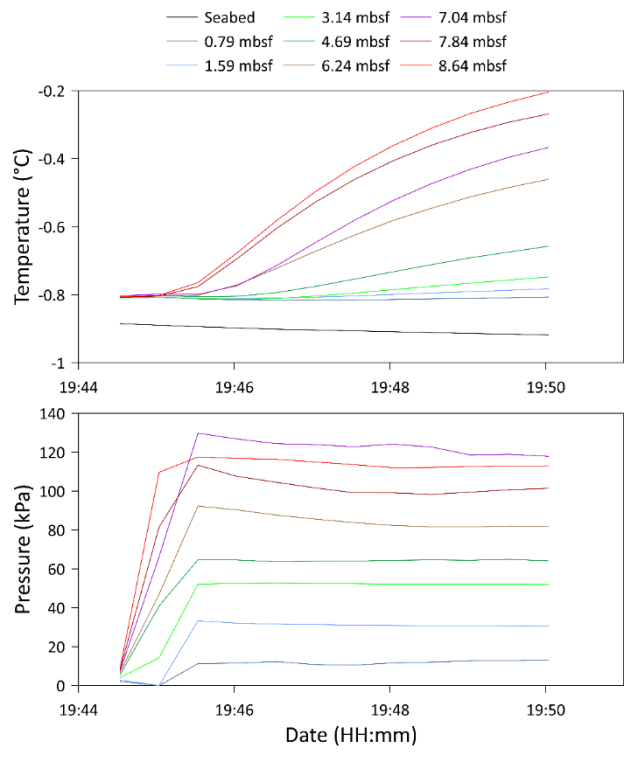
Figure 21. Data from piezometer site Str2-PZ2: Temperature and pore pressure variations during the installation of the piezometer.

Figure 22. Data from piezometer site Str2-PZ2: Temperature and pore pressure versus time. The different colors indicate the depth below the seabed. Sensor depths are between 0.79 mbsf (blue curve) and 8.64 mbsf (red curve).

Site CAGE20-6_KH_04_PZM2 (Str2-PZ4)

At site Str2-PZ4, the piezometer was deployed the 25/10/2020 to the east of Vestnesa ridge at water depth of 1127 m. Temperature and pore pressure variations during the installation of the piezometer are shown in Figure 23. The recorded data in Figure 23 indicate that the deployment was successful and the whole piezometer rod has penetrated the sediment between 22:07 and 22:08. The build-up pressure recorded by this piezometer is between 10 and 170 kPa (Figure 24).
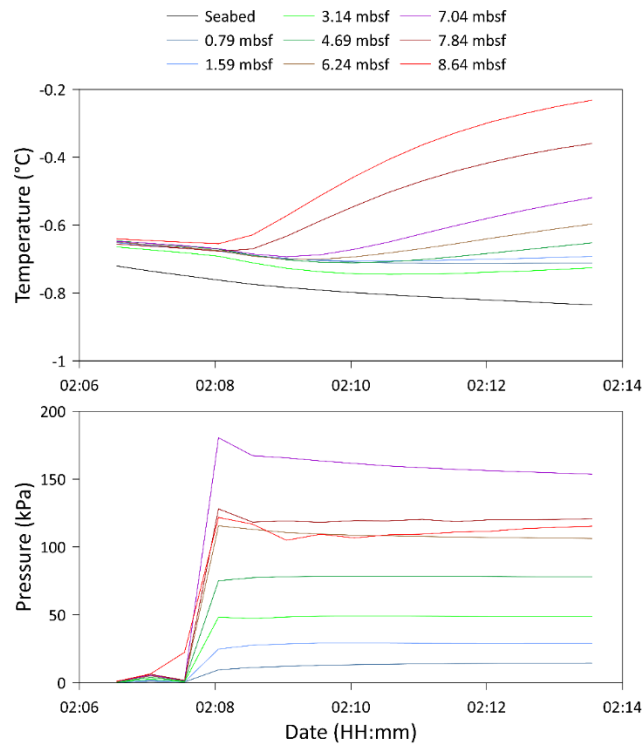
Figure 23. Data from piezometer site Str2-PZ4: Temperature and pore pressure variations during the installation of the piezometer.

Figure 24 indicates that the in-situ equilibrium temperature was reached 4 to 5 hours after the installation. The shape of the pore-pressure curves in Figure 24 indicates that the derivation of the in-situ equilibrium pore pressure will be not possible for some of the 8 sensors.
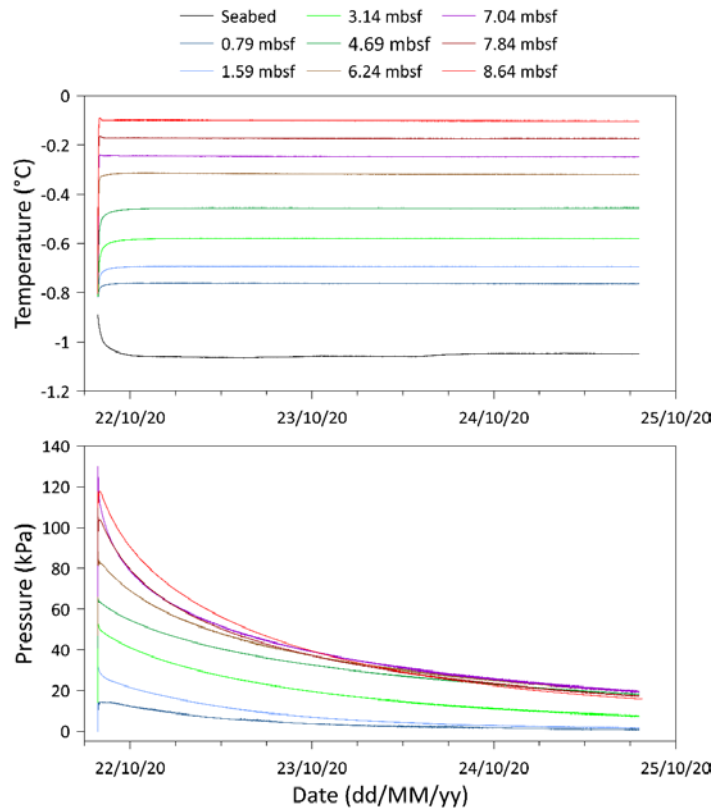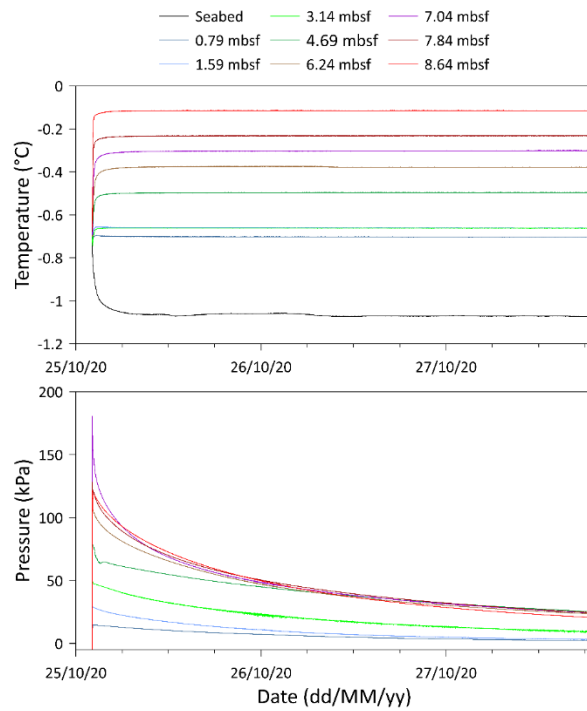
Figure 24. Data from piezometer site Str2-PZ4: Temperature and pore pressure versus time. The different colors indicate the depth below the seabed. Sensor depths are between 0.79 mbsf (blue curve) and 8.64 mbsf (red curve).

Summary Piezometer

Geothermal gradients obtained from the 4 piezometer sites are shown in Figure 25. The geothermal gradient is comparable between sites Str2-PZ1, Str2-PZ2 and Str2-PZ3 (between 89.9°C/km and 92°C/km) while it is 8% lower at site Str2-PZ4 (85.0°C/km).
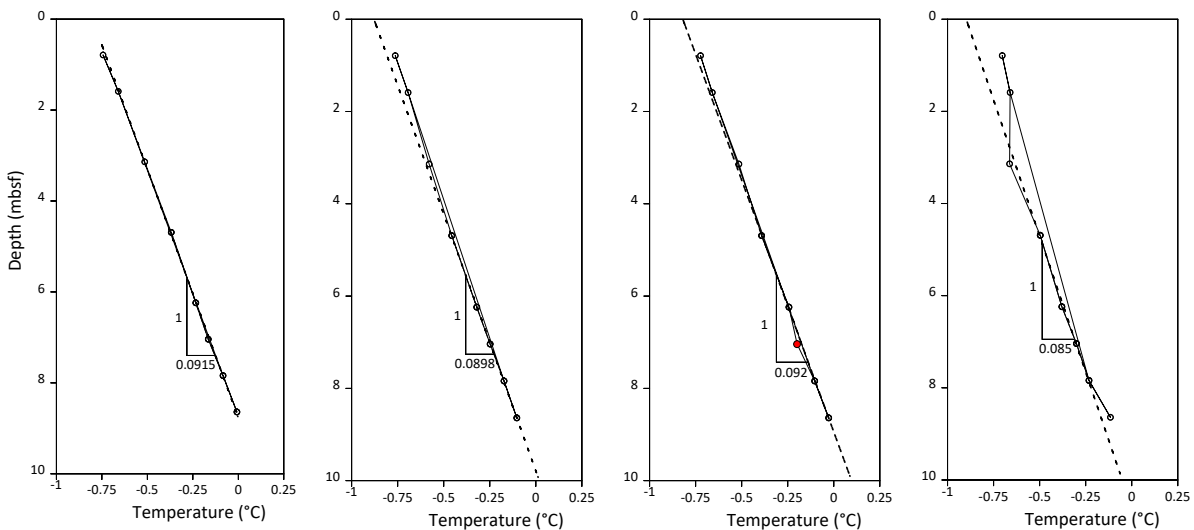
Figure 25. Geothermal gradients. From left to right: Str2-PZ1, Str2-PZ2, Str2-PZ3, Str2-PZ4.

Pore pressure build-up (Δui) during the installation process depends on the penetration rate and the stiffness and strength of the sediment. During the cruise, the penetration rate was imposed equal to 0.3 m/s. Therefore, any change of Δui can be attributed to the mechanical properties of the sediment. Δui obtained from the 4 piezometer sites are shown in Figure 26. Δui data are comparable between the two sites Str2-PZ1, Str2-PZ3 while Δui increases by around 20% at Str2-PZ2 and by more than 50% at site Str2-PZ4.
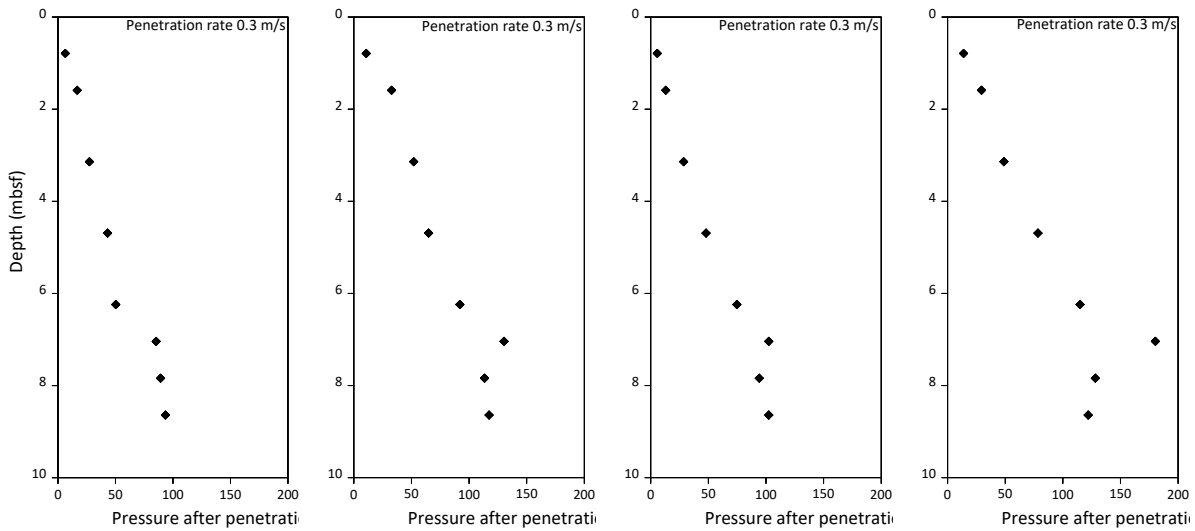
Figure 26. Pore pressure build-up (Δui) during the installation process. From left to right: Str2-PZ1, Str2-PZ2, Str2-PZ3, Str2-PZ4.

4.3 Super station 1 – Elongated depression between the beginning of the VR and the shelf break.

This feature started to get our attention during a Cage cruise in 2014 on board Helmer Hanssen, lead by Jürgen Mienert. We acquired acoustic data to check a site that was indicated as a gas flare/gas hydrate site in previous studies [e.g., *Sarkar et al.*, 2012; *Veloso-Alarcón et al.*, 2019] and in files with flare data from NOC Southampton. The elongated depression has smaller sub-depressions and vertical fluid flow features where massive hydrates were retrieved within the upper 2 meters of a gravity cores during CAGE17-5 cruise [*Andreassen et al.*, 2017] and reported by [*Sarkar et al.*, 2012]. Piezometer data acquired last year showed pressure and temperature pulses that suggest shallow gas migration during tides and sea level fluctuations [*Sultan et al.*, 2020]. A 12-penetration 'pogo-style' heat flow survey along the depression and 4 stations outside the depression were conducted to investigate any potentially anomalous heat regime inside the depression. We also collected 2 gravity cores over an area characterized by hummocky material on the seafloor (Figure 27). The location of the cores where carefully selected based on structures from the NKR 3D seismic volume and bathymetry maps available from CAGE20-5 cruise (Figure 27). The heat flow probe measurements show generally high heat flow within the depression than background stations, with particularly high thermal conductivities (mean of 1.3 W/mK) (e g., Figure 28). Within the depression the average thermal gradient was 85 ^{0}C/km, with a mean heat flow of 114 mW/m^2, compared to 91 ^{0}C/km and 103 mW/m^2 in the background stations (HF-21 to HF-24).
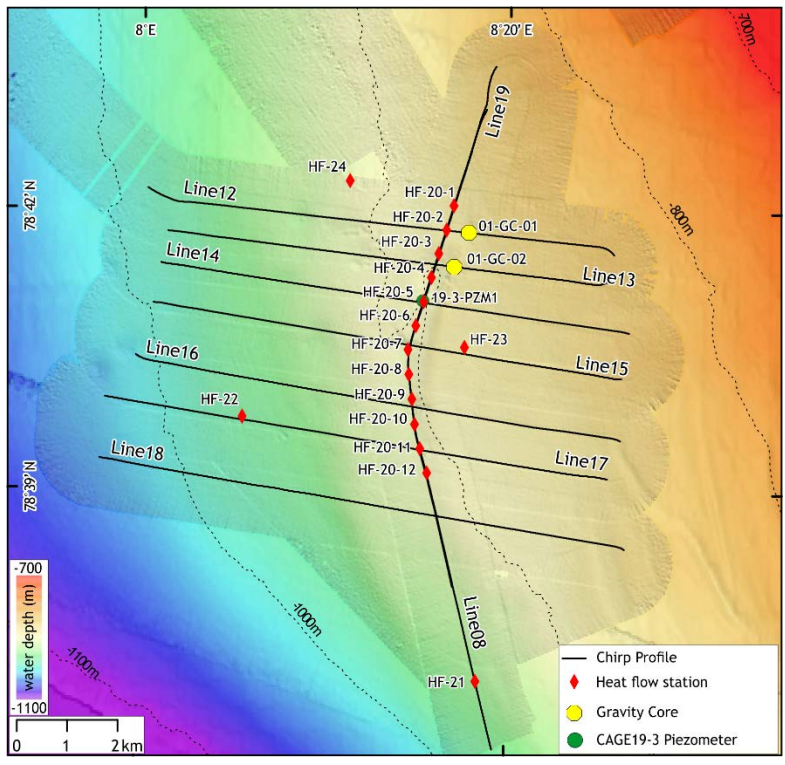
Figure 27 Bathymetry map and experiment design along the NKR (North Knipovich Ridge) elongated depression. Twelve heat flow stations are aligned inside the depression with a separation of 50 m. Two gravity cores were collected over hummocky seafloor at the flanks of vertical fluid flow features imaged in high resolution 3D seismic data. One sub-bottom profile line connects all the stations and 7 orthogonal lines were acquired for completing a pseudo 3D chirp survey (inline lines available from CAGE20-5 cruise).
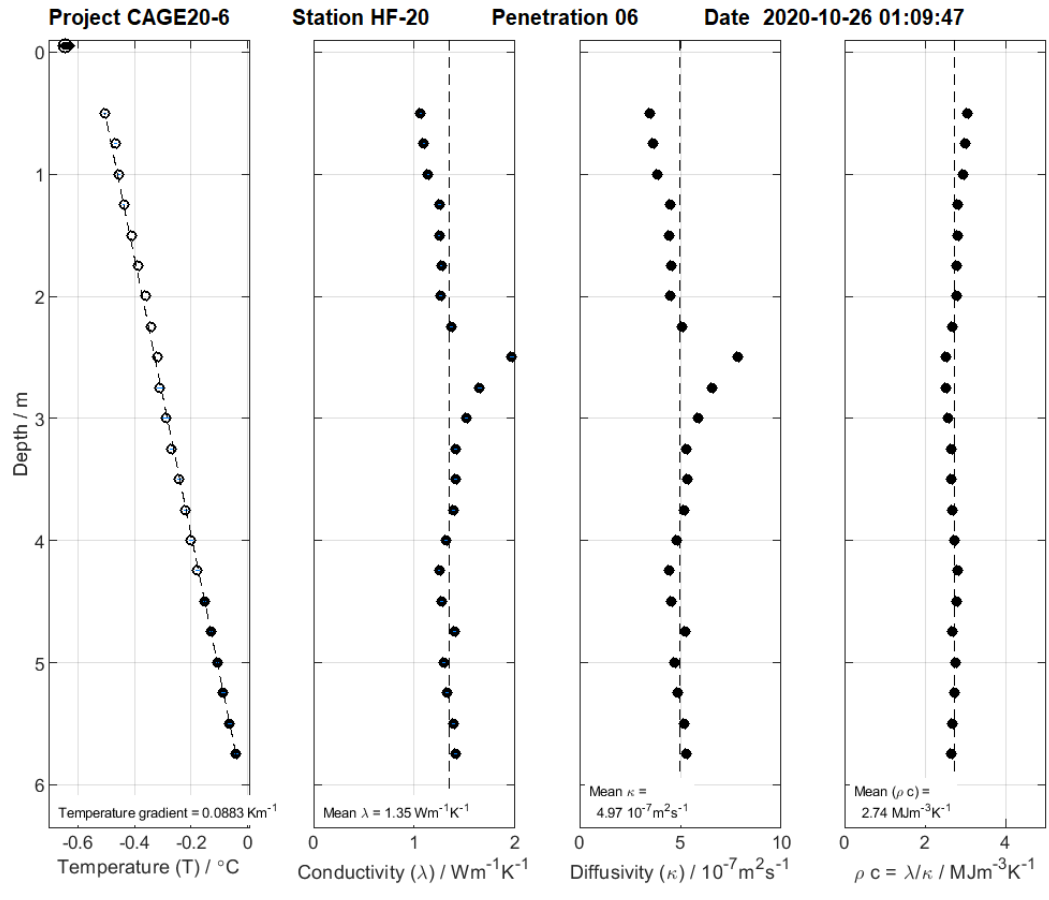
Figure 28 Plot of temperatures and thermal properties measured at station HF-20-6. Particularly high thermal conductivities were observed at 2.5m below the seafloor

4.4 Regional heat flow survey

We collected heat flow data from 22 stations distributed along the entire VR (Figure 7, HF-01 to HF-19, HF-25-HF-27). This was a regional survey to calculate background heat flow and further constrain BSR/gas hydrate stability dynamics and Molloy Ridge mid ocean spreading rates. The heat flow and thermal gradients show increasing trend towards the spreading centres with a mean thermal gradient in the region around 87 ^{0}C/km and mean heat flow of 100 mW/m^2. The highest thermal gradient in the region was observed at station HF-10 close to the Molloy Ridge (Figure 1), whereas heatflow show increasing trend toward the Molloy Transform Fault, with HF-06 recording a heat flow of ~144 mW/m^2 (Figure 28).
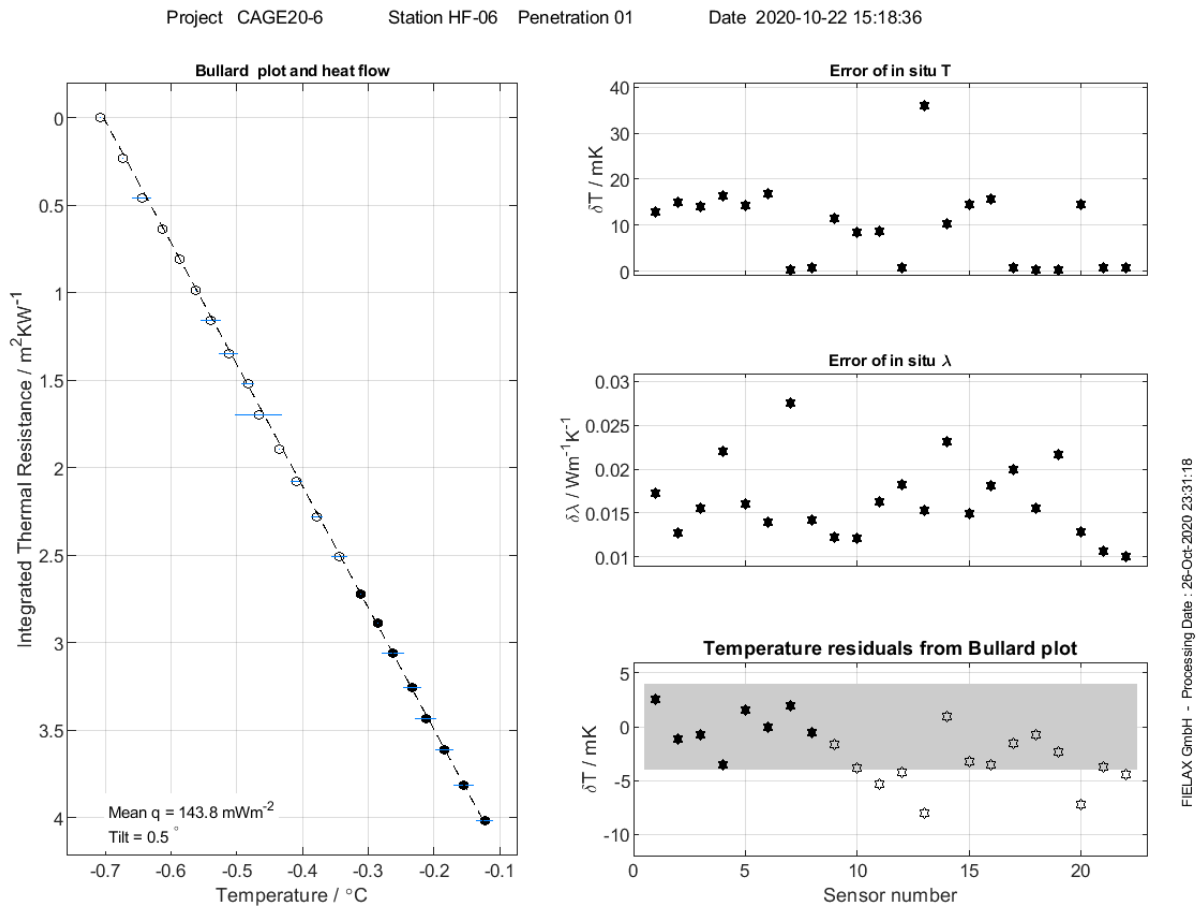
Figure 27 Bullard plot showing heat flow and errors in insitu measurements at station HF-06-01.

Acknowledgments

for their patience, enthusiasm and professionalism that made possible such technically challenging experiments in the Arctic. Thanks to the entire KH crew for making this an unforgettable experience.

Appendix - Cruise logs

Table A1 - Stations

Location	Station Id	Date	Time (UTC)	Lat. [N] Long. [E]	Penetration	Water Depth [m]	Notes
Vestnesa Ridge	CAGE20-6-KH-199-CTD	20.okt	12:42	79°03.769' 05°58.983'		1429	
Vestnesa Ridge	CAGE20-6-KH-12-PZM-01 - Dep	20.okt	18:22	79°07.242' 06°08.088'		1234	
Vestnesa Ridge	CAGE20-6-KH-04-GC-01	20.okt	21:56	79°00.305' 06°56.250'	133	1209	
Vestnesa Ridge	CAGE20-6-KH-04-GC-02	20.okt	23:31	79°00.286' 06°56.157'	433	1210	
Vestnesa Ridge	CAGE20-6-KH-04-OBS-01 - Dep	21.okt	03:48	78°59.865' 06°57.396'		1198	
Vestnesa Ridge	CAGE20-6-KH-04-OBS-02 - Dep	21.okt	09:02	79°00.023' 06°56.494'		1200	USBL did not release OBS (6:33 AM) and OBS came up in first attempt. OBS deployed again
Vestnesa Ridge	CAGE20-6-KH-04-OBS-03 - Dep	21.okt	11:37	79°00.127' 06°55.870'		1205	
Vestnesa Ridge	CAGE20-6-KH-04-OBS-05 - Dep	21.okt	14:11	79°00.379' 06°55.735'		1208	
Vestnesa Ridge	CAGE20-6-KH-04-OBS-04 - Dep	21.10.2020	17:02	79°00.203' 06°54.497'		1201	
Vestnesa Ridge	CAGE20-6-KH-04-PZM-01 - Dep	21.okt	19:47	79°00.285' 06°56.123'		1207	
Vestnesa Ridge	CAGE20-6-KH-01-HF-01	21.okt	20:56	79°01.536' 06°31.980'		1300	
Vestnesa Ridge	CAGE20-6-KH-01-HF-02	21.okt	22:26	79°01.536' 06°31.837'		1301.3	
Vestnesa Ridge	CAGE20-6-KH-01-HF-03	21.okt	22:50	79°01.536' 06°31.695'		1302.4	
Vestnesa Ridge	CAGE20-6-KH-02-HF-01	22.okt	01:24	79°01.849' 06°02.386'		1580	
Vestnesa Ridge	CAGE20-6-KH-02-HF-02	22.okt	02:52	79°01.850' 06°02.244'		1581	
Vestnesa Ridge	CAGE20-6-KH-02-HF-03	22.okt	03:14	79°01.875' 06°02.194'		1579	
Vestnesa Ridge	CAGE20-6-KH-03-HF-01	22.okt	05:04	79°05.375' 05°51.803'		1352	
Vestnesa Ridge	CAGE20-6-KH-03-HF-02	22.okt	06:15	79°05.385' 05°51.675'		1352	
Vestnesa Ridge	CAGE20-6-KH-03-HF-03	22.okt	06:45	79°05.396' 05°51.546'		1351	
Vestnesa Ridge	CAGE20-6-KH-04-HF-01	22.okt	08:20	79°06.855' 05°32.465'		1331	

Vestnesa Ridge	CAGE20-6-KH-04-HF-02	22.okt	09:27	79°06.859' 05°32.323'		1331	
Vestnesa Ridge	CAGE20-6-KH-04-HF-03	22.okt	09:59	79°06.863' 05°32.184'		1330	
Vestnesa Ridge	CAGE20-6-KH-05-HF-01	22.okt	11:43	79°07.563' 05°07.951'		1380	
Vestnesa Ridge	CAGE20-6-KH-05-HF-02	22.okt	12:50	79°07.537' 05°07.941'		1382	
Vestnesa Ridge	CAGE20-6-KH-05-HF-03	22.okt	13:14	79°07.511' 05°07.950'		1385	
Vestnesa Ridge	CAGE20-6-KH-06-HF-01	22.okt	14:52	79°03.442' 05°08.257'		1920	
Vestnesa Ridge	CAGE20-6-KH-06-HF-02	22.okt	16:04	79°03.446' 05°08.117'		1921	
Vestnesa Ridge	CAGE20-6-KH-06-HF-03	22.okt	16:28	79°03.449' 05°07.977'		1922	
Vestnesa Ridge	CAGE20-6-KH-07-HF-01	22.okt	18:21	79°04.255' 04°34.836'		2174.2	
Vestnesa Ridge	CAGE20-6-KH-07-HF-02	22.okt	19:43	79°04.280' 04°34.895'		2173	
Vestnesa Ridge	CAGE20-6-KH-07-HF-03	22.okt	20:07	79°04.304' 04°34.954'		2172	
Vestnesa Ridge	CAGE20-6-KH-08-HF-01	22.okt	22:01	79°09.328' 04°47.702'		1454.7	
Vestnesa Ridge	CAGE20-6-KH-08-HF-02	22.okt	23:13	79°09.301' 04°47.697'		1457	
Vestnesa Ridge	CAGE20-6-KH-08-HF-03	22.okt	23:37	79°09.274' 04°47.689'		1460	
Vestnesa Ridge	CAGE20-6-KH-09-HF-01	23.okt	00:59	79°10.529' 04°42.011'		1466	
Vestnesa Ridge	CAGE20-6-KH-10-HF-01	23.okt	03:10	79°11.567' 04°33.609'		1533	Second and third penetration without heat pulse failed due to damage to the battery cable
Vestnesa Ridge	CAGE20-6-KH-10-HF-02	23.okt	07:23	79°11.552' 04°33.626'		1533	Retry after fixing the battery cable. Recording stopped during the pull-out after the first penetration. No data from the two penetrations without heat pulse.
Vestnesa Ridge	CAGE20-6-KH-11-HF-01	23.okt	11:04	79°11.927' 05°02.155'		1475	Redeployed at the new station after recording data onboard.
Vestnesa Ridge	CAGE20-6-KH-11-HF-02	23.okt	12:14	79°11.902' 05°02.249'		1474	

Vestnesa Ridge	CAGE20-6-KH-11-HF-03	23.okt	12:37	79°11.877' 05°02.144'		1472	
Vestnesa Ridge	CAGE20-6-KH-12-GC-01	23.okt	17:20	79°06.747' 06°12.104'	512	1228.7	
Vestnesa Ridge	CAGE20-6-KH-12-PZM-01 - Rec	23.okt	20:05	79°07.216' 06°08.104'		1235	
Vestnesa Ridge	CAGE20-6-KH-12-PZM-02 - Dep	23.okt	23:00	79°06.747' 06°12.104'		1227.9	The time indicates the exact moment of insertion into the seafloor.
Vestnesa Ridge	CAGE20-6-KH-12-HF-01	24.okt	00:36	79°12.274' 05°30.857'		1499	
Vestnesa Ridge	CAGE20-6-KH-12-HF-02	24.okt	01:52	79°12.253' 05°30.749'		1498.1	
Vestnesa Ridge	CAGE20-6-KH-12-HF-03	24.okt	02:22	79°12.250' 05°30.881'		1497	
Vestnesa Ridge	CAGE20-6-KH-13-HF-01	24.okt	03:54	79°11.278' 05°59.652'		1381	
Vestnesa Ridge	CAGE20-6-KH-13-HF-02	24.okt	05:05	79°11.262' 05°59.756'		1380	
Vestnesa Ridge	CAGE20-6-KH-13-HF-03	24.okt	05:29	79°11.247' 05°59.875'		1379	
Vestnesa Ridge	CAGE20-6-KH-14-HF-01	24.okt	07:12	79°07.494' 06°29.470'		1379	
Vestnesa Ridge	CAGE20-6-KH-14-HF-02	24.okt	08:21	79°07.475' 06°29.570'		1378	
Vestnesa Ridge	CAGE20-6-KH-14-HF-03	24.okt	08:45	79°07.456' 06°29.674'		1378	
Vestnesa Ridge	CAGE20-6-KH-15-HF-01	24.okt	10:48	79°02.301' 06°58.842'		1287	
Vestnesa Ridge	CAGE20-6-KH-15-HF-02	24.okt	11:54	79°02.326' 06°58.815'		1287.4	
Vestnesa Ridge	CAGE20-6-KH-15-HF-03	24.okt	12:18	79°02.351' 06°58.789'		1288.2	
Vestnesa Ridge	CAGE20-6-KH-16-HF-01	24.okt	14:10	78°56.686' 06°31.563'		1613	
Vestnesa Ridge	CAGE20-6-KH-16-HF-02	24.okt	15:29	78°56.699' 06°31.697'		1610	
Vestnesa Ridge	CAGE20-6-KH-16-HF-03	24.okt	15:55	78°56.675' 06°31.638'		1612	
Vestnesa Ridge	CAGE20-6-KH-17-HF-01	24.okt	17:26	78°58.493' 06°54.450'		1255	
Vestnesa Ridge	CAGE20-6-KH-04-PZM-01 - Rec	24.okt	20:34	79°00.259' 06°56.139'		1208	
Vestnesa Ridge	CAGE20-6-KH-04-GC-03	24.okt	23:46	78°52.891' 07°28.596'	378	1127	
Vestnesa Ridge	CAGE20-6-KH-04-PZM-02 - Dep	25.okt	02:07	78°52.891' 07°28.596'		1127	The time indicates the exact moment of insertion into the seafloor.
Vestnesa Ridge	CAGE20-6-KH-04-OBS-rec	25.okt	04:45	79°00.683' 06°59.080'		1240	recovery
Vestnesa Ridge	CAGE20-6-KH-04-OBS-rec	25.okt	05:58	79°00.433' 06°57.578'		1220	
Vestnesa Ridge	CAGE20-6-KH-04-OBS-rec	25.okt	07:00	79°00.505' 06°56.740'		1218	

Vestnesa Ridge	CAGE20-6-KH-04-OBS-rec	25.okt	07:58	79°00.498' 06°54.852'		1210	
Vestnesa Ridge	CAGE20-6-KH-04-OBS-rec	25.okt	08:36	79°00.647' 06°55.880'		1217	
Vestnesa Ridge	CAGE20-6-KH-18-HF-01	25.okt	09:48	78°55.266' 07°09.232'		1226	
Vestnesa Ridge	CAGE20-6-KH-18-HF-02	25.okt	10:56	78°55.240' 07°09.238'		1226	
Vestnesa Ridge	CAGE20-6-KH-18-HF-03	25.okt	11:19	78°55.213' 07°09.243'		1227	
Vestnesa Ridge	CAGE20-6-KH-19-HF-01	25.okt	12:46	78°57.087' 07°27.891'		1198	
Vestnesa Ridge	CAGE20-6-KH-19-HF-02	25.okt	13:56	78°57.111' 07°27.854'		1198	
Vestnesa Ridge	CAGE20-6-KH-19-HF-03	25.okt	14:19	78°57.136' 07°27.818'		1198.6	No data was recorded
North Knipovich Ridge	CAGE20-6-KH-20-HF-01	25.okt	17:49	78°42.072' 08°16.998'		878	
North Knipovich Ridge	CAGE20-6-KH-20-HF-02	25.okt	19:16	78°41.816' 08°16.599'		883	
North Knipovich Ridge	CAGE20-6-KH-20-HF-03	25.okt	20:37	78°41.561' 08°16.202'		889.3	
North Knipovich Ridge	CAGE20-6-KH-20-HF-04	25.okt	22:01	78°41.304' 08°15.803'		903	recovered heat flow probe after 4th penetration at this site for data collection.
North Knipovich Ridge	CAGE20-6-KH-20-HF-05	25.okt	23:24	78°41.043' 08°15.392'		900	redeployed
North Knipovich Ridge	CAGE20-6-KH-20-HF-06	26.okt	01:09	78°40.786' 08°14.996'		905	
North Knipovich Ridge	CAGE20-6-KH-20-HF-07	26.okt	02:22	78°40.529' 08°14.590'		912	
North Knipovich Ridge	CAGE20-6-KH-20-HF-08	26.okt	03:44	78°40.266' 08°14.660'		907	
North Knipovich Ridge	CAGE20-6-KH-20-HF-09	26.okt	05:06	78°40.000' 08°14.828'		911	
North Knipovich Ridge	CAGE20-6-KH-20-HF-10	26.okt	06:33	78°39.734' 08°15.001'		911	
North Knipovich Ridge	CAGE20-6-KH-20-HF-11	26.okt	08:00	78°39.473' 08°15.286'		910	
North Knipovich Ridge	CAGE20-6-KH-20-HF-12	26.okt	09:28	78°39.217' 08°15.686'		909	
North Knipovich Ridge	CAGE20-6-KH-01-GC-01	26.okt	11:22	78°41.792' 08°17.819'	296	876	H2S smell (sulfide like odor)
North Knipovich Ridge	CAGE20-6-KH-01-GC-02	26.okt	12:45	78°41.419' 08°17.028'	377	875	H2S smell (sulfide like odor)
North Knipovich Ridge	CAGE20-6-KH-21-HF-01	26.okt	16:15	78°36.998' 08°18.437'		948	

Location	Line ID	Date	Time	Lat. [N] Long. [E]				Comments
North Knipovich Ridge	CAGE20-6-KH-21-HF-02	26.okt	17:19	78°37.018' 08°18.348'			948	
North Knipovich Ridge	CAGE20-6-KH-21-HF-03	26.okt	17:49	78°37.041' 08°18.259'			948	
North Knipovich Ridge	CAGE20-6-KH-22-HF-01	26.okt	19:03	78°39.800' 08°05.607'			970	
North Knipovich Ridge	CAGE20-6-KH-22-HF-02	26.okt	20:13	78°39.807' 08°05.729'			970	No data was recorded
North Knipovich Ridge	CAGE20-6-KH-22-HF-03	26.okt	20:38	78°39.816' 08°05.864'			969.4	No data was recorded
North Knipovich Ridge	CAGE20-6-KH-23-HF-01	26.okt	21:56	78°40.607' 08°17.757'			880	
North Knipovich Ridge	CAGE20-6-KH-23-HF-02	26.okt	23:04	78°40.582' 08°17.706'			880	
North Knipovich Ridge	CAGE20-6-KH-23-HF-03	26.okt	23:33	78°40.557' 08°17.653'			880	
North Knipovich Ridge	CAGE20-6-KH-24-HF-01	27.okt	00:42	78°42.331' 08°11.316'			909	Heat pulse not triggered
North Knipovich Ridge	CAGE20-6-KH-24-HF-02	27.okt	01:58	78°42.314' 08°11.441'			907	
North Knipovich Ridge	CAGE20-6-KH-24-HF-03	27.okt	02:27	78°42.314' 08°11.559'			906	
North Knipovich Ridge	CAGE20-6-KH-25-HF-01	27.okt	03:50	78°45.995' 07°58.899'			984	
North Knipovich Ridge	CAGE20-6-KH-25-HF-02	27.okt	05:02	78°45.973' 07°59.004'			983	
North Knipovich Ridge	CAGE20-6-KH-25-HF-03	27.okt	05:33	78°45.991' 07°59.109'			982	
Vestnesa Ridge	CAGE20-6-KH-12-PZM-rec	27.okt	11:15	79°06.747' 06°12.104'			1227	
Vestnesa Ridge	CAGE20-6-KH-04-PZM-rec	27.okt	20:30	78°52.891' 07°28.596'			1127	
Vestnesa Ridge	CAGE20-6-KH-24-HF-04	30.okt	08:00	78°42.406' 08°11.493'			910	
Vestnesa Ridge	CAGE20-6-KH-26-HF-01	30.okt	10:12	78°49.347' 07°43.100'			1065	
Vestnesa Ridge	CAGE20-6-KH-26-HF-02	30.okt	11:13	78°49.371' 07°43.046'			1065	
Vestnesa Ridge	CAGE20-6-KH-26-HF-03	30.okt	11:36	78°49.396' 07°42.990'			1066	
Vestnesa Ridge	CAGE20-6-KH-27-HF-01	30.okt	13:02	78°52.722' 07°29.193'			1126	
Vestnesa Ridge	CAGE20-6-KH-27-HF-02	30.okt	14:04	78°52.747' 07°29.138'			1126	
Vestnesa Ridge	CAGE20-6-KH-27-HF-03	30.okt	14:24	78°52.770' 07°29.085'			1126	

Table A2 – Acoustic lines

Location	Line ID	Date	Time (UTC) START	Lat. [N] Long. [E] START	Time (UTC) STOP	Lat. [N] Long. [E] STOP	Pulse mode	Ship Speed (kn)	Comments

Vestnesa Ridge	CAGE20-6-KH-01-CHIRP	20.10	14:05	79°05.594' 06°02.043'	14:44	79°08.248' 06°12.004'	Chirp	5	
Vestnesa Ridge	CAGE20-6-KH-02-CHIRP	20.10	15:03	79°07.545' 06°13.526'	15:31	79°07.182' 06°01.601'	Chirp	5	
Vestnesa Ridge	CAGE20-6-KH-03-CHIRP	20.10	15:55	79°07.896' 06°03.552'	16:22	79°06.692' 06°12.107'	Chirp	5	
Vestnesa Ridge	CAGE20-6-KH-04-CHIRP	20.10	20:04	79°00.771' 06°53.623'	20:17	79°00.032' 06°58.060'	Chirp	5	
Vestnesa Ridge	CAGE20-6-KH-05-CHIRP	20.10	20:27	79°00.647' 06°57.670'	20:43	78°59.748' 06°53.786'	Chirp	5	
Vestnesa Ridge	CAGE20-6-KH-06-CHIRP	23.10	15:13	79°04.902' 06°05.887'	15:58	79°07.981' 06°16.247'	Chirp	5	
Vestnesa Ridge	CAGE20-6-KH-07-CHIRP	24.10	22:04	78°55.566' 07°10.906'	23:10	78°51.985' 07°32.034'	Chirp	5	
North Knipovich Ridge	CAGE20-6-KH-08-CHIRP	26.10	14:04	78°43.522' 08°19.081'	15:42	78°36.413' 08°19.430'	Chirp	5	Line passing through the heat flow HF-20 stations
Vestnesa Ridge	CAGE20-6-KH-09-CHIRP	27.10	11:38	79°07.606' 06°16.899'	12:14	79°07.140' 06°01.326'	Chirp	5	
Vestnesa Ridge	CAGE20-6-KH-10-CHIRP	27.10	12:49	79°07.109' 06°00.899'	13:19	79°07.542' 06°13.470'	Chirp	5	
Vestnesa Ridge	CAGE20-6-KH-11-CHIRP	27.10	13:55	79°07.868' 06°03.615'	17:28	78°53.471' 07°26.482'	Chirp	5	
North Knipovich Ridge	CAGE20-6-KH-12-CHIRP	27.10	21:35	78°42.196' 08°00.540'	22:31	78°41.530' 08°25.837'	Chirp	5	
North Knipovich Ridge	CAGE20-6-KH-13-CHIRP	27.10	22:34	78°41.246' 08°25.094'	23:28	78°41.769' 08°01.422'	Chirp	5	
North Knipovich Ridge	CAGE20-6-KH-14-CHIRP	27.10	23:35	78°41.448' 08°00.842'	00:40	78°40.729' 08°26.554'	Chirp	5	
North Knipovich Ridge	CAGE20-6-KH-15-CHIRP	28.10	00:49	78°40.236' 08°26.069'	01:50	78°41.002' 08°00.776'	Chirp	5	
North Knipovich Ridge	CAGE20-6-KH-16-CHIRP	28.10	02:02	78°40.429' 07°59.848'	03:10	78°39.565' 08°26.256'	Chirp	5	
North Knipovich Ridge	CAGE20-6-KH-17-CHIRP	28.10	03:19	78°39.181' 08°25.137'	04:27	78°39.993' 07°58.069'	Chirp	5	
North Knipovich Ridge	CAGE20-6-KH-18-CHIRP	28.10	04:41	78°39.326' 07°58.158'	05:52	78°38.412' 08°26.451'	Chirp	5	
North Knipovich Ridge	CAGE20-6-KH-19-CHIRP	28.10	06:21	78°38.043' 08°17.076'	07:27	78°43.238' 08°19.210'	Chirp	5	

References

Andreassen, K., P. Henry, and t. s. crew (2017), Marine Geophysical Cruise   to the Yermak Plateau and western Svalbard continental margin*Rep.*, https://cage.uit.no/cruise-logs/.

Crane, K., E. Sundvor, R. Buck, and F. Martinez (1991), Rifting in the northern Norwegian-Greenland Sea: Thermal tests of asymmetric spreading, *Journal of Geophysical Research: Solid Earth (1978–2012)*, *96*(B9), 14529-14550.

Himmler, T., D. Sahy, T. Martma, G. Bohrmann, A. Plaza-Faverola, S. Bünz, D. J. Condon, J. Knies, and A. Lepland (2019), A 160,000-year-old history of tectonically controlled methane seepage in the Arctic, *Science advances*, *5*(8), eaaw1450.

Johnson, J. E., J. Mienert, A. Plaza-Faverola, S. Vadakkepuliyambatta, J. Knies, S. Bünz, K. Andreassen, and B. Ferré (2015), Abiotic methane from ultraslow-spreading ridges can charge Arctic gas hydrates, *Geology*, G36440. 36441.

Knies, J., S. Vadakkepuliyambatta, and S. crew (2019), Calypso giant piston coring in the Atlantic-Arctic gateway – Investigation of continental margin development and effect of tectonic stress on methane release*Rep.*, CAGE-UiT, https://cage.uit.no/cruise-logs/.

Lister, C., J. Sclater, E. Davis, H. Villinger, and S. Nagihara (1990), Heat flow maintained in ocean basins of great age: investigations in the north-equatorial west Pacific, *Geophysical Journal International*, *102*(3), 603-630.

Plaza-Faverola, A., and M. Keiding (2019), Correlation between tectonic stress regimes and methane seepage on the western Svalbard margin, doi:https://doi.org/10.5194/se-10-79-2019.

Plaza-Faverola, A., S. Vadakkepuliyambatta, W. L. Hong, J. Mienert, S. Bünz, S. Chand, and J. Greinert (2017), Bottom-simulating reflector dynamics at Arctic thermogenic gas provinces: An example from Vestnesa Ridge, offshore west Svalbard, *Journal of Geophysical Research: Solid Earth*, *122*(6), 4089-4105.

Sarkar, S., C. Berndt, T. A. Minshull, G. K. Westbrook, D. Klaeschen, D. G. Masson, A. Chabert, and K. E. Thatcher (2012), Seismic evidence for shallow gas-escape features associated with a retreating gas hydrate zone offshore west Svalbard, *Journal of Geophysical Research: Solid Earth*, *117*(B9), doi:10.1029/2011JB009126.

Schneider, A., G. Panieri, A. Lepland, C. Consolaro, A. Crémière, M. Forwick, J. E. Johnson, A. Plaza-Faverola, S. Sauer, and J. Knies (2018), Methane seepage at Vestnesa Ridge (NW Svalbard) since the Last Glacial Maximum, *Quaternary Science Reviews*, *193*, 98-117.

Sultan, N., and S. Lafuerza (2013), In situ equilibrium pore-water pressures derived from partial piezoprobe dissipation tests in marine sediments, *Canadian Geotechnical Journal*, *50*(12), 1294-1305.

Sultan, N., A. Plaza-Faverola, S. Vadakkepuliyambatta, S. Buenz, and J. Knies (2020), Impact of tides and sea-level on deep-sea Arctic methane emissions, *Nature Communications*, *11*(1), 1-10.

Veloso-Alarcón, M. E., P. Jansson, M. De Batist, T. A. Minshull, G. K. Westbrook, H. Pälike, S. Bünz, I. Wright, and J. Greinert (2019), Variability of acoustically evidenced methane bubble emissions offshore western Svalbard, *Geophysical Research Letters*, *46*(15), 9072-9081.